

Spring 2015

Aqueous foam stabilized by tricephalic Amphiphilic surfactants

Seth A. Heerschap
James Madison University

Follow this and additional works at: <https://commons.lib.jmu.edu/honors201019>

 Part of the [Chemistry Commons](#), and the [Physics Commons](#)

Recommended Citation

Heerschap, Seth A., "Aqueous foam stabilized by tricephalic Amphiphilic surfactants" (2015). *Senior Honors Projects, 2010-current*. 104.
<https://commons.lib.jmu.edu/honors201019/104>

This Thesis is brought to you for free and open access by the Honors College at JMU Scholarly Commons. It has been accepted for inclusion in Senior Honors Projects, 2010-current by an authorized administrator of JMU Scholarly Commons. For more information, please contact dc_admin@jmu.edu.

Aqueous Foam Stabilized by Tricephalic Amphiphilic Surfactants

by

Seth Heerschap

A thesis submitted in fulfillment of the requirements for the JMU Honors Program



James Madison University
May, 2015

© Copyright by Seth A. Heerschap 2015
All Rights Reserved

Accepted by the faculty of the Department of Physics and
Astronomy, James Madison University, in partial fulfillment of the
requirements for the Honors Program.

FACULTY COMMITTEE:

Klebert Feitosa, Ph.D.,
Assistant Professor, Department of Physics and Astronomy

Kevin Caran, Ph.D.,
Associate Professor, Department of Chemistry

Brian Utter, Ph.D.,
Associate Professor, Department of Physics and Astronomy

Philip Frana, Ph.D.,
Interim Director, Honors Program

Abstract

Aqueous foams can be described as a close packing of gas bubbles stabilized by surface active molecules. Their complex and diverse properties make them attractive for many chemical and physical applications where foaming, emulsifying or coating processes are needed. The recent synthesis of multi-cephalic and multi-tailed amphiphilic molecules have reportedly [1] enhanced their antibacterial activity in connection with tail length and nature of the head group.

This report covers the foamability of two triple head, double tail cationic surfactants (M-1,14,14, M-P,14,14) and a triple head single tail cationic surfactant (M-1,1,14) and compares them with commercially available single headed, single tailed anionic and cationic surfactants (SDS, CTAB and DTAB). Additionally, a longer tailed variant (M-1,16,16) was also tested.

The results show that bubble rupture rate decreases with the length of the carbon chain, irrespective of head structure. For the longer tailed variant (M-1,16,16) foam was difficult to produce leaving it untestable. The growth rate of bubbles with short tailed surfactants (SDS) and longer, single tailed tricationic surfactants (M-1,1,14) was shown to be twice as high as those with longer tailed surfactants (CTAB, M-P,14,14, M-1,14,14). This fact was related to the size variation of bubbles, where the foams made with short tail surfactants exhibited higher polydispersity than those with short tails. This suggests that foams with tricationic amphiphilics are closely linked to their tail length and generally insensitive to their head structure.

Acknowledgements

First and foremost, I would like to thank my research advisor, Dr Klebert Feitosa, for his continuous support during the past year and a half. Without his help and bookkeeping none of this would have been possible, he was always available for help when I needed it most. I'm glad to have been able to have the opportunity to work with him on such a project.

Thanks to my labmates, Keely Criddle, Olivia Cypull and Dan Shorts for being a fun and supportive! In particular, Keely, for making the conference trip to South Carolina possible.

I appreciate Dr Caran for his collaboration allowing this project to be attainable using his exotic surfactants. Thanks for all the lab tricks, the basic lab training and for the willingness to answer all of my chemistry (and non-chemistry) related questions.

Thanks to Dr Caran's lab assistants, Kristin McKenna, John Marafino and Brenna for their help in synthesizing the molecules I was able to use for experiments.

Thanks to Dr Harry Hu, who graciously aided me in machining several of the parts and the countless rheometer support.

Thanks to Mr Philips and Dr Butner for their encouraging words and interest in my future. I'm also grateful to my parents and my sisters for their encouragement and support in these past two years.

Special thanks to the JMU physics department for making research such a priority and allowing students, like me, the opportunity to discover...

Contents

1	Introduction	8
1.1	Motivation	8
1.2	A Stable Foam	9
1.3	Unique Surfactants	12
1.4	Evolving Foam	14
2	Description of Research	15
3	Experimental Process	15
3.1	Foam production	15
3.1.1	The Device	16
3.1.2	Foam Production, Device Specifications and Creation	19
3.1.3	Foam Creation Specifications	21
3.2	Imaging Foam	22
3.2.1	Refracting Imaging Technique	23
3.2.2	Sample Placement and Sealing	28
3.2.3	Imaging/Camera Specifications	28
3.3	Image Analysis	29
4	Results	35
4.1	Sodium Dodecyl Sulfate (SDS)	35
4.2	Dodecyl Trimethyl Ammonium Bromide (DTAB)	40
4.3	Cetyltrimethylammonium Bromide (CTAB)	41

4.4	M-1,14,14	44
4.5	M-P,14,14	46
4.6	M-1,16,16	49
4.7	M-1,1,14	49
4.8	Comparing Results	52
	4.8.1 Bubble Count	52
	4.8.2 Coarsening and Polydispersity	54
4.9	Uncertainty and Assumptions	56
5	Conclusions	57
6	Outlook	59

List of Figures

1	Van Der Waal Attractions	9
2	Sodium Stearate	10
3	Surfactants at liquid-air interfaces	11
4	Novel Synthesized Surfactants	13
5	Commercial Surfactants used	13
6	Foam production Cartoon	17
7	Foam production image	17
8	Microfluidic device - general view	18
9	Microfluidic device - overhead	18
10	Microfluidic device - layout	19
11	Microfluidic device - schematic	20
12	Microfluidic device - ‘in action’	23
13	Imaging setup	24
14	Refractive filtering - Cartoon	25
15	Refractive filtering - resulting effect	26
16	Refractive filtering - image	27
17	Image analysis - original image	29
18	Image analysis - corrected for distortion	30
19	Image analysis - contrasting and bubble counting	31
20	Sauter and average radius compared (a)	32
21	Sauter and average radius compared (b)	33
22	Individual bubbles through time	34

23	Effect of different concentrations - average radius	36
24	Effect of different concentrations - number of bubbles	37
25	Bubble number for SDS	38
26	Sauter radius for SDS	38
27	Polydispersity for SDS	39
28	Foam evolution images for SDS	39
29	Bubble number for DTAB	40
30	Foam evolution images for DTAB	41
31	Bubble number for CTAB	42
32	Sauter radius for CTAB	42
33	Polydispersity for CTAB	43
34	Foam evolution images for CTAB	43
35	Bubble number for M-1,14,14	44
36	Sauter radius for M-1,14,14	45
37	Polydispersity for M-1,14,14	45
38	Foam evolution images for M-1,14,14	46
39	Bubble number for M-P,14,14	47
40	Sauter radius for M-P,14,14	47
41	Polydispersity for M-P,14,14	48
42	Foam evolution images for M-P,14,14	48
43	Bubble number for M-1,1,14	50
44	Sauter radius for M-1,1,14	50
45	Polydispersity for M-1,1,14	51

46	Foam evolution images for M-1,1,14	51
47	Bubble number for all surfactants	52
48	Sauter radius for most surfactants	53
49	Polydispersity for most surfactants	53
50	Growth rates for each recorded surfactant	55
51	Number of initial bubbles versus Critical Micelle Concentration . . .	55
52	Ideal Solids and Fluids	61
53	A Complex Fluid	63

1 Introduction

1.1 Motivation

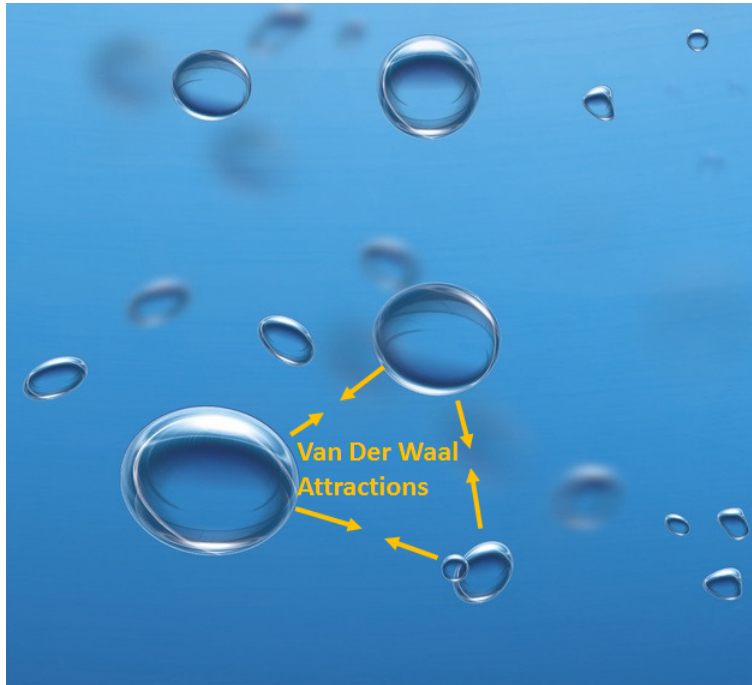
The recent advances in science are highlighted by today's healthy and rich lifestyle. These advances are made possible only by better understanding the physical world. One common trend in history is that further research unveils even more complexities and research opportunities. An excellent example of is the science of complex fluids.

In the past few decades there has been a plethora of research and new technologies opening up new areas of research. Areas that previously were very difficult or impossible to examine. One subset of these complex fluids is foams. This will be the chief topic of this paper.

Some of the motivation behind the study of foams is their wide range of applications. For example, fire retardants require a high surface area to liquid ratio to cover fuel and prevent fire from spreading; foam fulfills this condition perfectly. Foam contains surface active agents (surfactants), giving it the ability to mediate the difference between hydrophilic and hydrophobic materials. This is used in household soaps, shampoo and cleaners to pick up oil and dirt easily. The ability to separate materials also makes it useful in the mining industry. A process known as froth flotation has made possible material recovery from very low grade ore. In fact, about 80% of all materials mined benefit from this process [2].

This paper will focus on understanding the physics of foam and how it is related to its corresponding stabilizing molecules. Recently, a new family of these surfactant molecules was synthesized by the work of Dr Caran's research group. The surfactants were found to contain a unique molecular architecture which has been found to display antibacterial resistance against pathogenic bacteria [3,4]. By combining the anti-bacterial abilities of these surfactants with the cleaning properties of foam, an effective multi-purpose cleaning product may be a possibility.

Figure 1: Van Der Waal Attractions



This figure shows the natural, van der Waal, attractions of air bubbles in water.

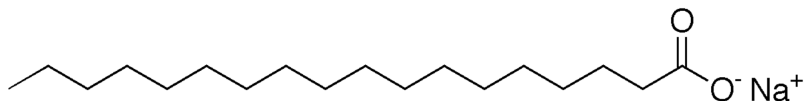
1.2 A Stable Foam

Aqueous foam* is made of gas or air that is trapped in a liquid [8,11]. Foams can be created in nearly any liquid substance by mixing in gas. For example, shaking a bottle of water creates foam lasting about a second or two. A closer look at these gas bubbles would reveal individual molecules linked together to form a sphere with the inside being air and the outside surrounded by liquid. An example of this is seen in Figure 1.

For pure substances such as water, foams rarely last long and are usually unstable. To minimize its energy, solutions naturally attempt to minimize their surface area, this causes foam to ultimately dissipate away until there are no bubbles left. This “principle of least action” is more apparent in fluids with higher surface tension and

*A complex foam. See Appendix for a more formal introduction and definition

Figure 2: Sodium Stearate



Sodium Stearate, a common surfactant molecule found in many commercial products.

thus are less stable. The molecular charge plays a role. Van der Waal attractions between the gas interface of the bubbles also destabilize the foam. These attractions pull the gas bubbles together (Figure 1). Eventually the bubbles are close enough so that there is only a thin film of separation, with no structure and only attraction this film loses its stability and breaks causing the bubble to rupture.

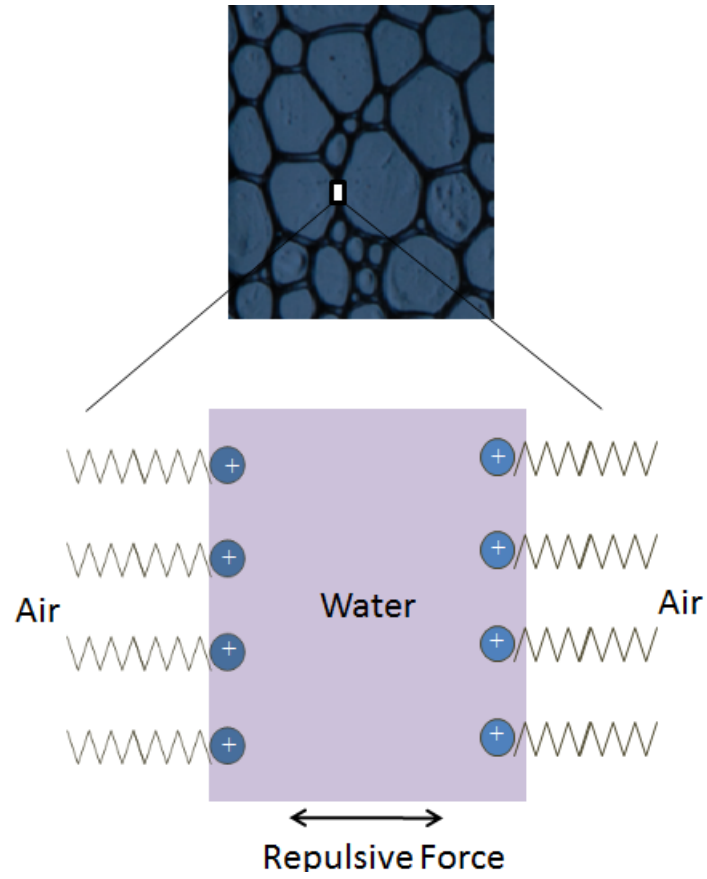
By adding in a small amount of soap to water, stable aqueous foam can be made. Foam originating from this soapy water mix lasts days and even weeks without dissipating. The major stabilizing molecule in this soap is its surfactants.

The surfactants, or surface active agents, are amphiphilic molecules, containing a hydrophobic (oil-loving) hydrocarbon tail on one end of the molecule and a hydrophilic (water-loving) head at the other. Surfactants are commonly found in pharmaceuticals, pesticides and detergents. Figure 2 shows a drawing of sodium stearate, a common surfactant found in many commercial soaps and deodorants.

When added to water, these molecules minimize their free energy by aligning themselves at air-water interfaces [9]. As seen in Figure 3, the hydrophilic heads (water-loving) will stick into the solution while the hydrophobic tails (oil-loving) stick out into the air. The alignment of the molecules at the interface produce lower, more lateral electrostatic forces resulting in reduced surface tension. This property makes them useful in several applications, in particular, for agricultural sprays where their wetting ability enhances pesticide activity on the leaves of plants [1,7,8].

Foams containing surfactants gain their stability from the repulsive nature of these amphiphiles. Comparable to water, the van der Waals attractions pull the gas bubbles together. Unlike water, this force is canceled out by the repulsive electrostatic force from the polar side of the surfactant molecules, (i.e. like charges repel, see Figure 3) and the reduced surface tension derived from the surfactant molecules.

Figure 3: Surfactants at liquid-air interfaces



This cartoon shows the alignment of surfactant molecules along two liquid-air interfaces.

Thus, surfactants improve the stability of foam by preventing the bubbles from being torn apart [11].

Another notable feature of surfactants is micelle formation. When the surfactant concentration in the solution reaches a critical point ϕ_{CMC} , the tails of the molecule cannot escape the water and instead form an enclosure with the heads pointing out and the tails pointing inward [1,11]. These tiny enclosures are known as micelles. The CMC of these molecules depends greatly on the chemical composition and architecture of the surfactant molecules. For example, longer tailed amphiphilic molecules generally require a lower concentration of molecules to form micelles than shorter tailed surfactants [1,3]. This property makes it an interest for this paper. It can be theorized that this relation extends to the foaming properties of different surfactant stabilized solutions.

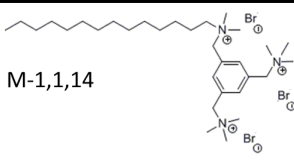
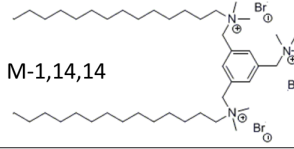
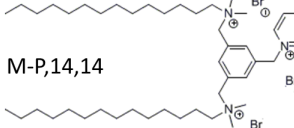
1.3 Unique Surfactants

The stabilizing molecule for aqueous foam, the surfactant, can take many different forms [10]. For example, there are cationic, anionic and non-ionic hydrophilic heads and different length hydrophobic tails. As one might expect, this is likely to affect foam evolution and rheological properties [13].

Recently, Dr. Kevin Caran's research group has been able to synthesize a very different architecture of amphiphilic molecules. Where most surfactants contain a single hydrophilic head and a hydrophobic tail, they were able to form surfactants with two or three ammonium head groups and one or two tails [1,3,4]. Figure 4 lists some of the tricephalic (triple headed) amphiphiles synthesized by Dr Caran's group. The architecture of these molecules can be compared to the commercial surfactants (see Figure 5).

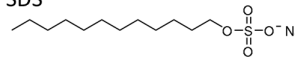
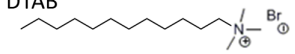
Applications using this unique structure are currently being investigated. In particular, bicephalic (double headed) amphiphiles have been shown to affect antibacterial activity among pathogenic bacteria [4]. An added benefit of this structure is its method of crippling the cell. Unlike many antibodies, the polycephalic structure allows the molecule to attack specifically the cell membrane, rendering it hard for

Figure 4: Novel Synthesized Surfactants

Abbrev. Name	Mass (g/mol)	Tail	CMC	Drawing
M-1,1,14 M-1,1,16 M-1,1,18	716.56 744.61 772.66	14 16 18	21 mM 11 mM 5.0 mM	M-1,1,14 
M-1,10,10 M-1,12,12 M-1,14,14 M-1,16,16 M-1,18,18	786.69 842.80 898.90 955.01 1011.1	10 12 14 16 18	12 mM 2.5 mM .61 mM .16 mM **	M-1,14,14 
M-P,10,10 M-P,12,12 M-P,14,14 M-P,16,16 M-P,18,18	806.68 862.78 918.89 975.00 1031.1	10 12 14 16 18	14 mM 2.4 mM .56 mM .18 mM **	M-P,14,14 

This table shows several of the surfactants synthesized by Dr Caran's Lab. The names highlighted in red were used in this study, all of which had a head charge of +3.

Figure 5: Commercial Surfactants used

Abbrev. Name	Mass (g/mol)	Tail	Head Charge	CMC (mM)	Drawing
SDS	288.38	12	-1	8.20	SDS 
DTAB CTAB	308.34 364.46	12 16	+1	15.3 0.96	DTAB 

the cell to develop antibacterial resistance [4,14].

1.4 Evolving Foam

Simple fluids and solids are generally time independent; their texture and properties do not change over time. Quartz, for example, keeps its crystalline structure for many years. Froths and foams containing mineral stabilizers show similar behavior [12]. Aqueous foam is different since its structure is constantly changing with time. There are three main processes which can be observed: bubble coarsening, drainage and film rupture.

Coarsening is the exchange of air traveling from bubbles of high pressure to low pressure. Due to surface tension, the gas bubble's pressure is inversely proportional to its radius. This leads to a net flux of gas from small bubbles to big bubbles. Thus, bubbles that are smaller than their nearest neighbors get smaller at an increasing rate while the neighboring bubbles will grow. Since the smaller bubbles disappear, the overall rate of increase of the average size will be proportional to its coarsening rate. Given enough time, the foam will ultimately end its life by evolving into a complete separation between liquid and gas.

Drainage is the process by which gravity pulls the liquid downward. Over time, bubbles at the top become drier with thinner films; this causes the bubbles to become more polyhedral with distinct angles and edges (see Figure 21 for an example of this). Towards the bottom, the bubbles remain wet due to the capillary action from the sides of the container pulling the aqueous solution upward, countering the gravitational forces which normally would pull the water further downward.

Film rupture is a byproduct of drainage. When bubble films become thin and dry enough, there is no water to stabilize the surfactants, ultimately they pop. The gap illustrated in Figure 3 becomes thin and this causes the films to inevitably rupture.

2 Description of Research

The goal in this research is to better understand how molecular architecture in surfactants affect the physics of the foam. To a small extent there has been research studying different surfactant molecules and their corresponding effect on foam rheology [13,15]. However, there has been a limited investigation linking different molecular structures to the corresponding physics of the foam.

This paper will investigate coarsening and rupture rates of aqueous foams (water and surfactant only) stabilized by a range of different structured surfactants. Three different, common, commercial surfactants were tested: Sodium dodecyl sulfate (SDS), Cetyltrimethylammonium bromide (CTAB) and Dodecyl trimethyl ammonium bromide (DTAB). In addition, this study examined foam made from several of Dr Kevin Caran’s unique amphiphilic surfactants labeled: M-1,14,14, M-P,14,14, M-1,1,14 and M-1,16,16. While drainage was not examined directly in this study, it affected the coarsening and rupture rates, particularly after several hours.

This data provides a better understanding of foam coarsening and rupture and its connection with individual molecular makeup. With several different surfactant architectures tested, a model correlating microscopic geometry with physical properties can be obtained.

3 Experimental Process

Understanding coarsening and rupture of different foam requires several experimental steps: Foam production, foam imaging and finally image and data analysis. Each process had a unique set of challenges associated with it, as described in the next section.

3.1 Foam production

In order to accurately compare the properties of different foams, the production method must aim to create foams with a constant “foamability” and texture. “Foam-

ability” is defined by the number of bubbles per unit area of a highly monodisperse foam. Highly “foamable” foam, for example, would have a high volume density of nearly monodisperse bubbles.

There are three independent variables; each of which can be controlled:

- Initial size of the bubbles, Initial Sauter radius (R_{32}).
- Size variation, polydispersity (PDI).
- Concentration of surfactant-water solution (ζ).

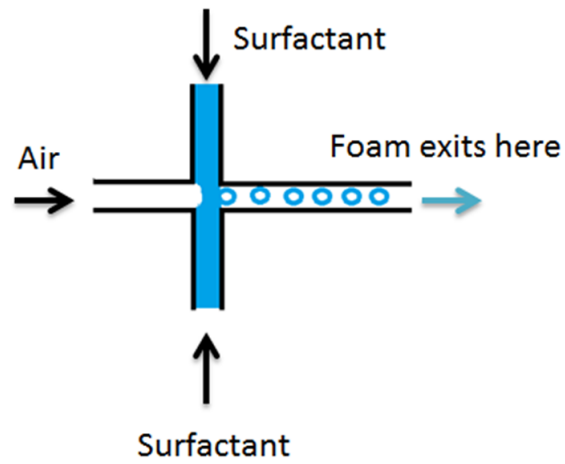
Any of these variables can be controlled by changing the way the foam is made [13]. Here we chose to make the foam using a micro-fluidic device. The size can be adjusted by adjusting the speed at which the solution and air mix; a higher mixture speed can create smaller bubbles, this makes sense since these bubbles have a higher pressure. Polydispersity is harder to control. A desirable monodisperse would have a polydispersity of zero ($PDI = 0$). By using a pump that supplies a constant air injection with constant solution injection, the polydispersity can be minimized. The third variable, concentration, is the easiest to control since it is simply the amount of solute in the solution.

3.1.1 The Device

The first goal was to build a device that could create monodispersed bubbles by pumping a constant air pressure, mixing the solute and solvent. Due to the scarcity of the tricephalic surfactants, only a limited amount was available for experimentation. A microfluidic device addressed this problem by producing foam from very small amounts of liquid [16]. In this device, two small streams of surfactant, driven by a syringe pump, were mixed with a similar stream of air. The resulting mixture exiting the device, was a precise foam which could be placed in a container for later imaging. A cartoon showing this mixing setup is shown in Figure 6.

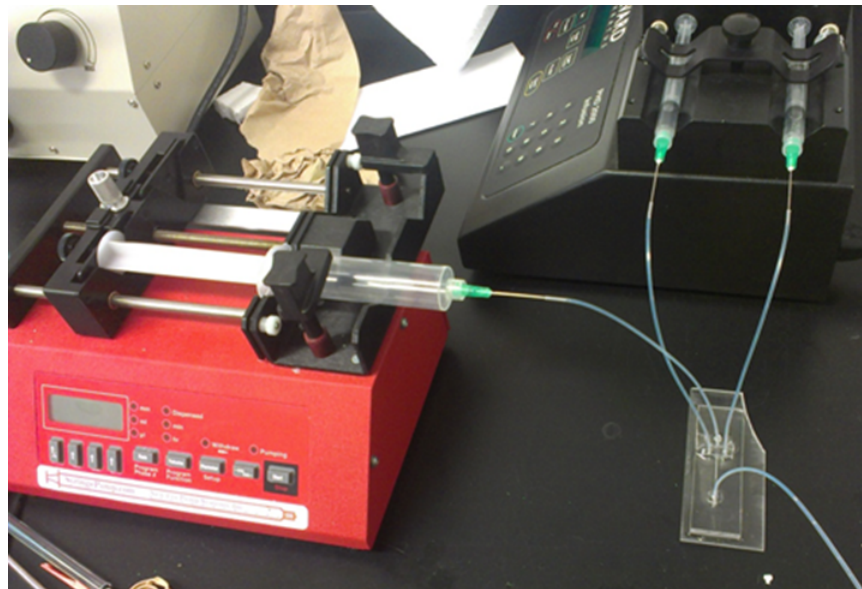
Figure 7 shows this “mini-foam machine” fully connected to the syringe pumps, the black pump containing the surfactant and the red pump containing air.

Figure 6: Foam production Cartoon



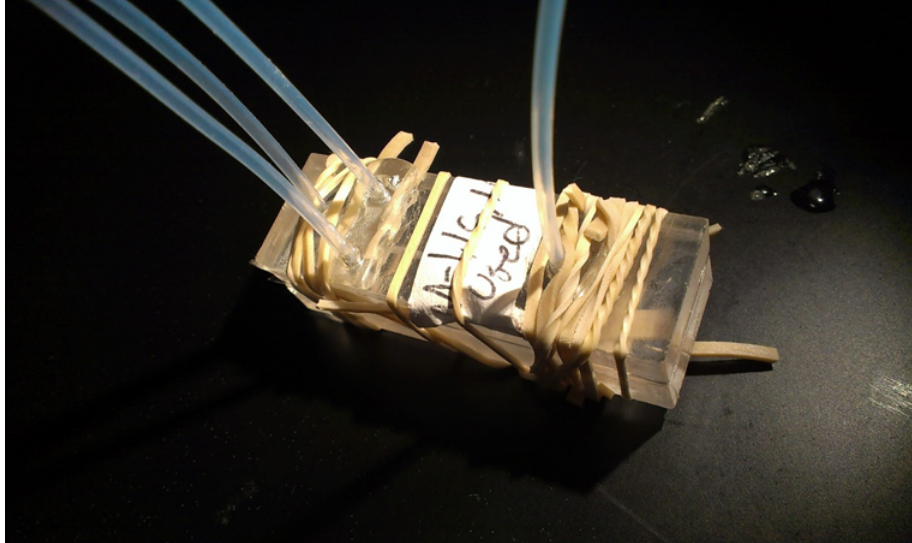
This cartoon shows how the surfactant solution and air were mixed.

Figure 7: Foam production image



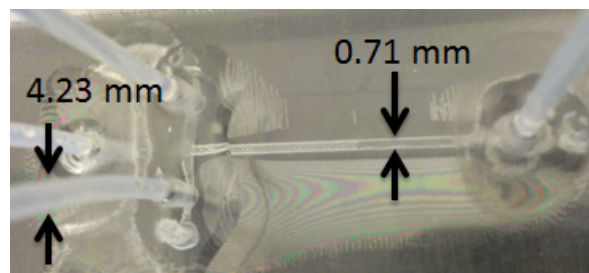
This image shows one of our older foam-making devices. The air from the red syringe pump mixes with the two syringes from the black pump to create foam a foam exiting out the fourth tube.

Figure 8: Microfluidic device - general view



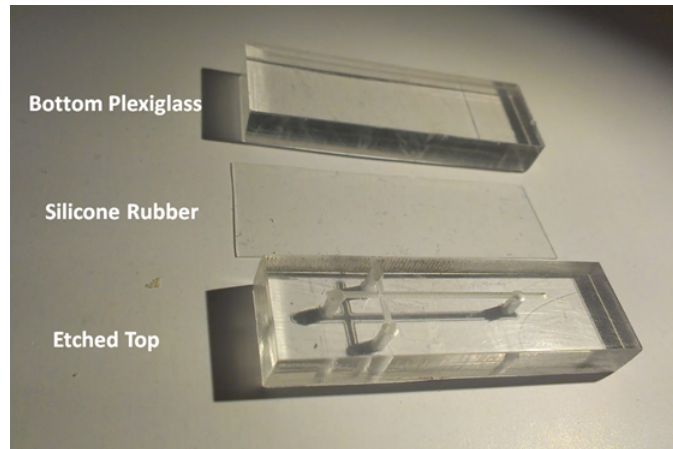
This image shows a close-up of one of the actual devices used. We found that rubber bands with a rubber seal prevented liquid from escaping at higher pressures than solely UV activated glue as used in Figure 7.

Figure 9: Microfluidic device - overhead



This image shows an overhead view of the device. It should be noted that the extra drilled hole towards the bottom left is a mistake, however, this did not affect the foaming process.

Figure 10: Microfluidic device - layout



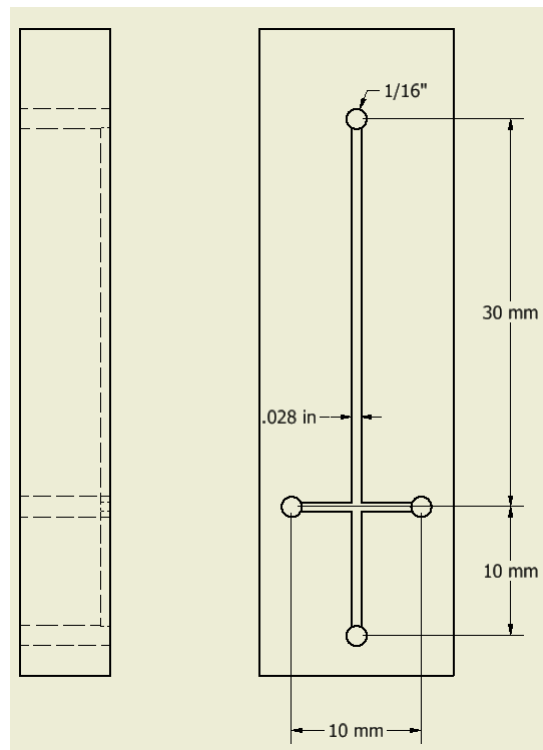
This image shows a layout of the parts. With little adhesive needed the device could easily be cleaned and sandwiched back together. Figure 8 shows the complete assembly.

Figures 8 and 9 show a close-up of the device. In Figure 9 the fluid paths and etchings can be observed. Figure 10 shows each cut part laid out.

3.1.2 Foam Production, Device Specifications and Creation

The procedure for creating this device is as follows: By using a VersaLaser (carbon laser) printer, the channels are etched into plexiglass (as shown in the schematic, Figure 11). Next, four 1/16th inch holes were drilled which intersected the channels. A piece of transparent silicone rubber was layered on top of the etched region sealing it off. A piece of plexiglass with identical dimensions of the first is placed on top of the rubber sealant, the block is then secured by rubber bands holding the “sandwich” together. 1/16th inch tubing was used for the piping. Four tubings were cut approximately 25 cm in length with one being cut at a flat, 90 degree angle and the second end cut at a 45 degree angle. The second end of the tubing is then inserted into the drilled holes with the sharp part of the tube oriented away from channels allowing flow. Finally to prevent leakage, a UV activated adhesive was used to seal the pipings and holes together.

Figure 11: Microfluidic device - schematic



Created using AutoDesk inventor, this drawing shows the dimensions of the microfluidic device. The depth was purposely not included since plexiglass of several different depth were used. The depth of the cut was also unknown and varied depending on the power of the laser.

3.1.3 Foam Creation Specifications

To provide an accurate comparison between foams, the texture and foamability of the foams had to start out similar to each other. With the foaming device, there were three different variables that could be adjusted: Surfactant concentration, injection velocity and liquid to air ratio. An ineffective method of foam creation might add error when comparing the different surfactant molecules. Thus, each of these variables are carefully examined.

The first test was determined to find the optimal concentration of surfactant in the water. Several different concentrations were tested in four separate trials using Sodium dodecyl sulfate (SDS) surfactant mixed with distilled water. The concentrations chosen were: 0.200, 0.100, 0.050 and 0.025 Molar concentrations. The mixtures were each vigorously shaken and placed together at roughly the same time, as they aged, several images were taken to compare foam heights. The results of this experiment showed that the 0.100M and 0.200M concentrations proved to be easy to produce foam (good foamability) and showed good stability (foam lasting several hours). By contrast, the 0.050M and 0.025M foams disappeared significantly faster and proved harder to make by simple shaking. Thus, the 0.100M solution was chosen for its low surfactant concentration, good foamability and stability.

The “optimal” 0.100M concentration that was used for the SDS stabilized foam did not work when using different surfactant molecules. It was realized through experimentation, that concentration alone was not a satisfying gauge on stability and foamability. The structure, mass and shape of the molecule all affected these properties. The solution proposed involved using a constant Critical Micelle Concentration (CMC) from molecule to molecule. This is more accurate than the concentration alone since the CMC takes into account the size and shape of the molecule. For example, the double tailed M-1,14,14 amphiphiles require only a small concentration (0.00061M) to create micelles, whereas single tailed molecules required a concentration about eight times higher [3].

As experimentally determined, the CMC of SDS is about 0.0082M [17], thus the 0.01M concentration leading to good foamability was about 12.2 times the CMC

(12.2x CMC). Throughout the rest of the paper it is assumed that 12.2x CMC is the optimal foamability of all surfactant solutions tested. This assumption could be an area of investigation in future experiments.

The second variable integrated was the injection velocity. Initially it was determined that the injection velocity did not affect the size in bubbles (visibly). Thus, all of the experiments were performed with the same injection velocity specifications:

This variable wasn't examined in detail since it did not seem to change the size of the bubbles (visibly). It wasn't until after most of the experiments were performed that differences in bubble size was observed from surfactant to surfactant.

- Air: 76.156 mL/hr
- 2 X Surfactant each at 5.905 mL/hr

Later it was observed that small variations in pumping speed did alter the size of the bubbles, but a detailed investigation will be the topic of future experiments.

The final variable is the air to liquid ratio or liquid fraction (ϕ_{LF}). Essentially, how wet or dry the foam is. This ratio was calculated by:

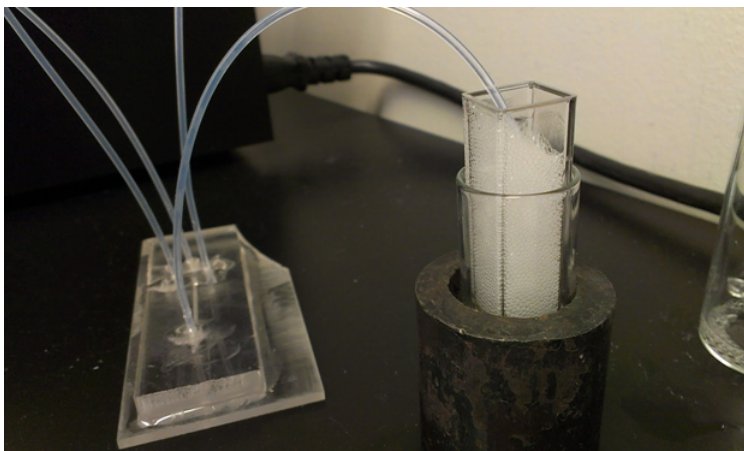
$$\phi_{LF} = \frac{2V_{surf}}{2V_{surf} + V_{air}} \quad (1)$$

For all foams, with one exception explained in a later section, the same ratio of 0.134 calculated from equation 2 was created. This constant was determined by trial and error using SDS and DTAB solutions; once established, no further liquid fraction tests were made.

3.2 Imaging Foam

The most suitable container for foam imaging is a small, cubical container. Curved glass containers create a distortion. Spectrophotometer cuvettes fit this criteria perfectly being well sized and transparent. Figure 12 shows the foaming device filling up the cuvette. For all imaging, a Nikon D200 camera was used with the AF-S Micro NIKKOR 105mm f/2.8 lens and all auto stabilization off. For lighting, two separate

Figure 12: Microfluidic device - ‘in action’



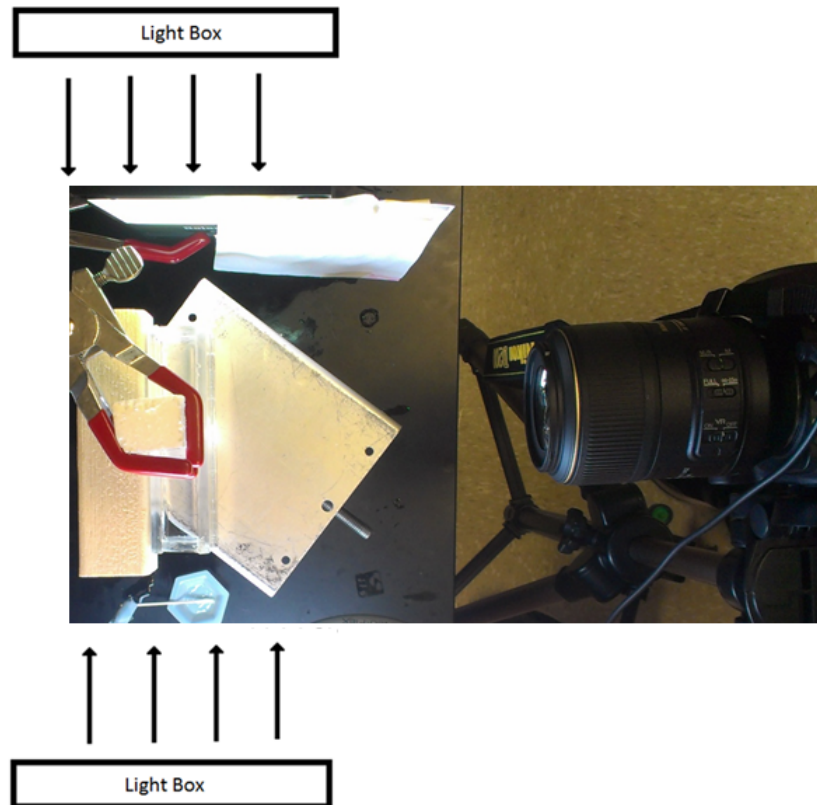
This image shows the foam-maker in action. Generally it took about two minutes to fill the cuvette (volume = 4.74cm^3).

sources, a fluorescent panel and LED panel, were used to provide lighting at two different angles as shown in Figure 13 and 16. It should be noted that the two light sources used emitted slightly different color light, this added an extra step in the image analysis.

3.2.1 Refracting Imaging Technique

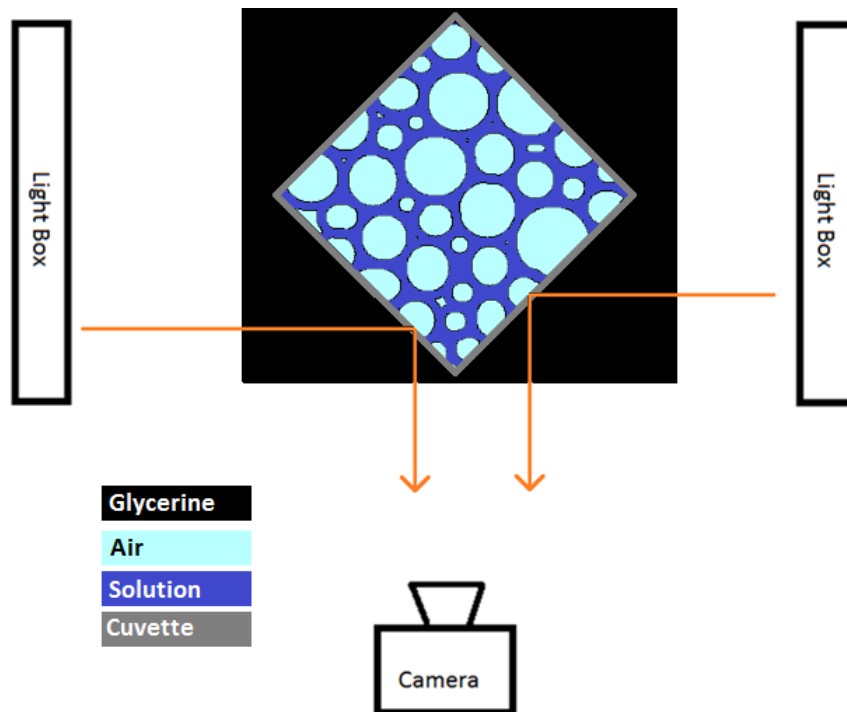
Using an imaging technique developed by A. E. Roth et al [18] an effective imaging technique was found by exploiting Snell’s Law, contrasting the higher refractive liquid with the lower refractive air. Consider the illustration in Figure 14. After passing into the high refractive index glycerine substance, the light then passes into the cuvette container. If there is an air bubble at this point, the index refraction difference (between the air the glycerine) is great enough for total internal reflection (TIR) to happen, the light is then reflected into the lens of the camera. However, if the light entering the cuvette strikes an area in which water solution is touching the container, the difference in index of refraction is too small for TIR and the light passes through. This refractive contrasting can be seen in Figure 15. The camera and lighting setup can be seen in Figures 16 and 13.

Figure 13: Imaging setup



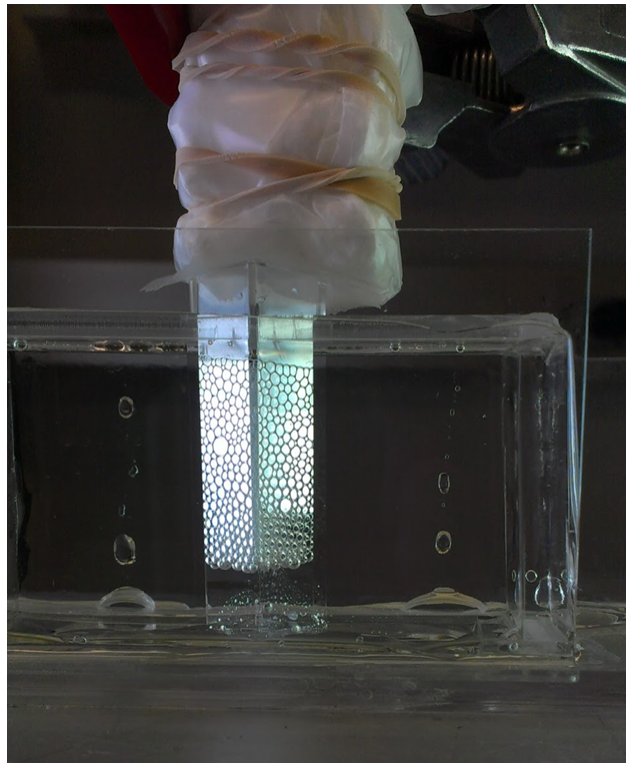
An overhead view of the setup. The sample is illuminated by two light sources, an LED source located at the top of the image and a fluorescent panel located at the bottom (not shown). The camera distance varied from experiment to experiment.

Figure 14: Refractive filtering - Cartoon



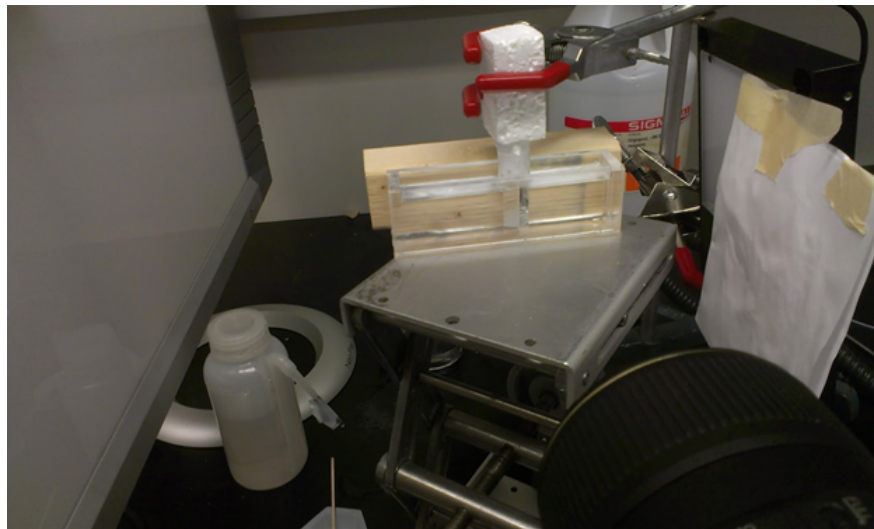
This cartoon shows an overhead view of the refractive setup. Light coming from the two sources enter the glycerine. When the light passes into the cuvette it is separated. Light that strikes an air bubble is totally internally reflected out to the camera. Light striking the solution passes through.

Figure 15: Refractive filtering - resulting effect



This example image is the result of the refractive filtering shown in Figure 14. Since this image was not taken exactly at a 45 degree angle, there are slight refractive inconsistencies, especially on the bottom right of the cuvette. Image taken by HTC 4 MP camera.

Figure 16: Refractive filtering - image



This image shows an alternate view of the experimental setup. It was determined that the lighting distance from the sample didn't affect the imaging. The spread from the lighting was eliminated by taping paper over the light sources (seen on the right side, but not the left). The lights in the room were also left on and didn't noticeably affect image quality.

Glycerine has an index of refraction of 1.473, thus the critical angle of TIR between it and air is:

$$\sin^{-1}\left(\frac{n_{air}}{n_{Glycerine}}\right) = 42.76 \text{ degrees} \quad (2)$$

Since this angle is less than 45 degrees, by orienting the container at a 45 degree angle light from both sides is internally reflected back to the camera; allowing twice as much data to be collected each shot. For reference, water to air has a critical angle greater than 45 degrees, preventing the ability to collect data from both sides simultaneously.

3.2.2 Sample Placement and Sealing

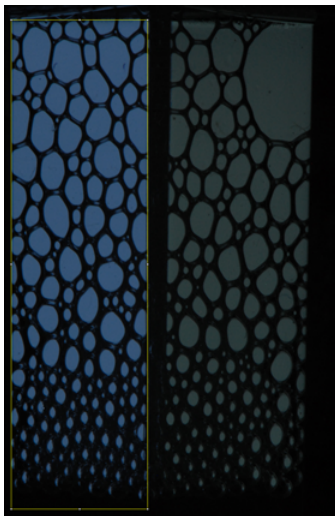
The glycerine containment box was created using machined plexiglass with UV activated sealant. For optimal visibility and scratch resistance, the front panel, originally plexiglass, was replaced with glass, this avoided the problem of small scratches affecting image quality. In Figure 15 this containment wall is partially visible.

Once the cuvette had been filled, it was quickly sealed with scotch tape to prevent glycerine and other contaminants in. To keep the sample from floating in the glycerine and to reinforce the seal, a metal clamp pushing down a parafilm wrapped styrofoam block was used as shown in Figures 16 and 15.

3.2.3 Imaging/Camera Specifications

With the sample secured, lit up and positioned at a 45 degree angle, camera imaging could begin. As seen in Figure 13, the camera was secured with a tripod about 200 cm from the sample (the actual distance is of minimal importance, as long as the whole cuvette could be imaged). Since the cuvette was at a 45 degree angle a small F-Number (F-Stop) was used (usually F45) to guarantee a wide depth of field. With the F-Number held constant, image lighting was controlled by varying the shutter speed. For example, if the lights in the room were turned on, the shutter speed would be increased to adjust for the same imaging intensity.

Figure 17: Image analysis - original image



The original image from the Nokia camera. Note the different color lighting on each side: Left, florescent lighting, right, LED lighting.

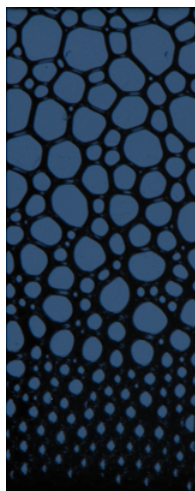
To observe the foam evolution, images were taken at equal intervals with a time resolution of two minutes for a total time ranging from 200 to 400 minutes depending on the rupture and coarsening rate. In most situations after about 200 minutes nearly all of the bubbles had disappeared and the remaining few would last days prolonged by the capillary forces from the edges of the cuvette. Stable foams lasting about 200 minutes are the main attention of this paper and the two minute resolution was sufficient. Unstable foams, such as DTAB stabilized, which quickly dissipated were tested, however, they were not the focus of this paper and would have required a much better time resolution in order to accurately study.

3.3 Image Analysis

The purpose of image analysis was to find the area and location of each bubble in all images. All image analysis was performed using ImageJ, a Java-based image processing software. The following is step by step procedure of the process.

A sample of the image taken by the camera is shown in Figure 17. Because

Figure 18: Image analysis - corrected for distortion



The distortion in this image is corrected. This was done by stretching and cropping the image.

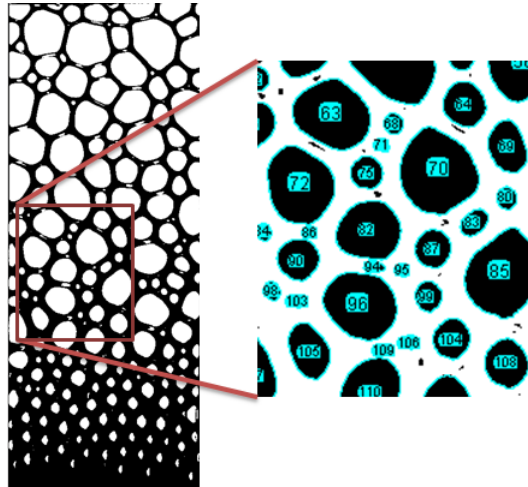
the lighting sources emitted slightly different wavelength light (LED more orange, florescent bluer), each side had to be analyzed separately.

In addition, each experimental run had to be scaled separately. This was because the camera was placed at slightly different distances from the sample each run. Scaling was performed by measuring the width of the cuvette in pixels and then converting it to millimeters since the physical width of the cuvette was known (≈ 10 mm). Because the cuvette was tilted at a 45 degree angle there was about a $(10 \text{ mm}) * \sin(45) \approx 7$ mm difference in distance from the front and the back. It can be observed in several of the images (for example Figures 17, 20 and 21) that there is a slight angling of the top due to this distance. This distortion was considered insignificant and ignored in calculations.

Since the cuvette was tilted at a 45 degree angle, the image appeared distorted. This was easily corrected by stretching the image horizontally by a factor of $\sqrt{2}$. Figure 18 shows the result for the left side.

With the appropriate, undistorted image, analysis was possible. The image was then converted to 8-bit and a threshold was applied, contrasting the bubbles out. Using ImageJ's built in area counter, the area, location, circumference, circularity

Figure 19: Image analysis - contrasting and bubble counting



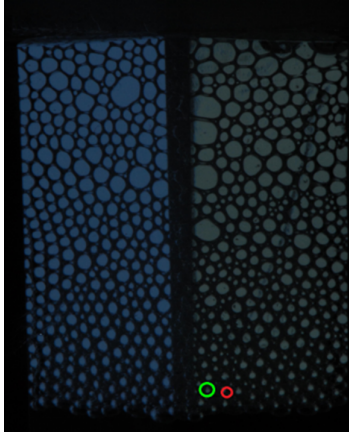
The last two steps of the image analysis process. The image is converted to 8-bit then contrasted to get the image on the left. By using ImageJ's built in area counter the size, location, circularity, etc, of each bubble could be determined as seen on the left image. Note that the numbers on each bubble are the bubble number; not the area.

and centroid of each bubble could be determined. A visual aid for this process is shown in Figure 19. To help filter out unwanted shapes, only bubbles with a circularity of greater than 0.4 and an area of larger than 300 pixels (roughly 0.15 mm) were counted. A macro was created to automate the process and looped for all image stacks. This was repeated for the left side to complete the image analysis for each experiment.

This method of image analysis allows relatively easy bubble tracking since the location and size of each bubble for every frame is known. However, the two minute time resolution was not suited for this type of analysis. In the complex nature of foam there exists many quick rearrangements which are only observable when using a high speed camera.

The bubble radius was determined for a circular bubble of the equivalent measured area. This calculation was performed for all the bubbles. The foam evolution was then determined by observing how the radius of the bubbles changed from picture to picture. The red line in Figure 22 shows the average bubble radius of M-P,14,14

Figure 20: Sauter and average radius compared (a)



A sample of SDS stabilized foam newly made, note the low polydispersity. The red and green circles display the average area and the Sauter mean radius respectively. The Sauter mean radius (green) shows a better representation of size than the purely average (red).

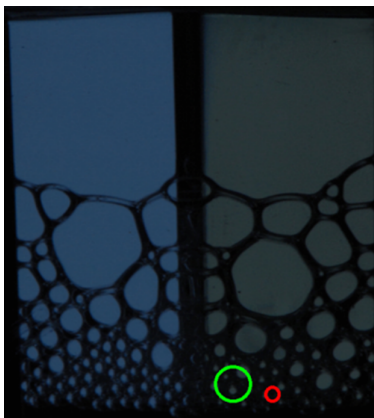
foam as a function of time. Note that the average size increases. Due to coarsening, there was a divergent behavior between the few growing bubbles and the large amount of shrinking bubbles. This caused the average size to be an inaccurate representation of overall bubble size. This can be seen by the red circle in Figures 20 and 21, note how it appears to the eye far too small.

To give a better representation of size, the Sauter mean radius was used given by equation 4:

$$R_{Sauter} = \frac{\sum_n^N R_n^3}{\sum_n^N R_n^2} = \frac{\langle R^3 \rangle}{\langle R^2 \rangle} \quad (3)$$

With N being the total number of bubbles counted for every n th bubble. This value provides more accurate information than the average because the larger bubbles are given more weight. As seen in Figures 20 and 21, the mean Sauter radius, in green, gives a better representation of size than the purely average radius in red. This value also makes sense theoretically because when dealing with three dimensional coarsening, the rate of change of the volume $\langle R^3 \rangle$ is proportional to its surface area $\langle R^2 \rangle$ [19]. For this paper, the initial Sauter radius of the bubbles ranged from 0.7 to

Figure 21: Sauter and average radius compared (b)



This image uses the same foam as Figure 20 but at a later time. Note how the Sauter radius (green) increases. The bottom bubbles remain small due to the capillary action from the sides of the container pulling the liquid upwards keeping the films thick.

1.7 mm (reference Figure 48).

This data was then graphed, as seen in Figure 22 for the aqueous foam stabilized by a M-P,14,14 surfactant. Each dot represents individual bubble at a certain time. Note the largest bubble starting at about 2.6 mm at $t = 0$ and growing to nearly 7 mm at $t = 300$.

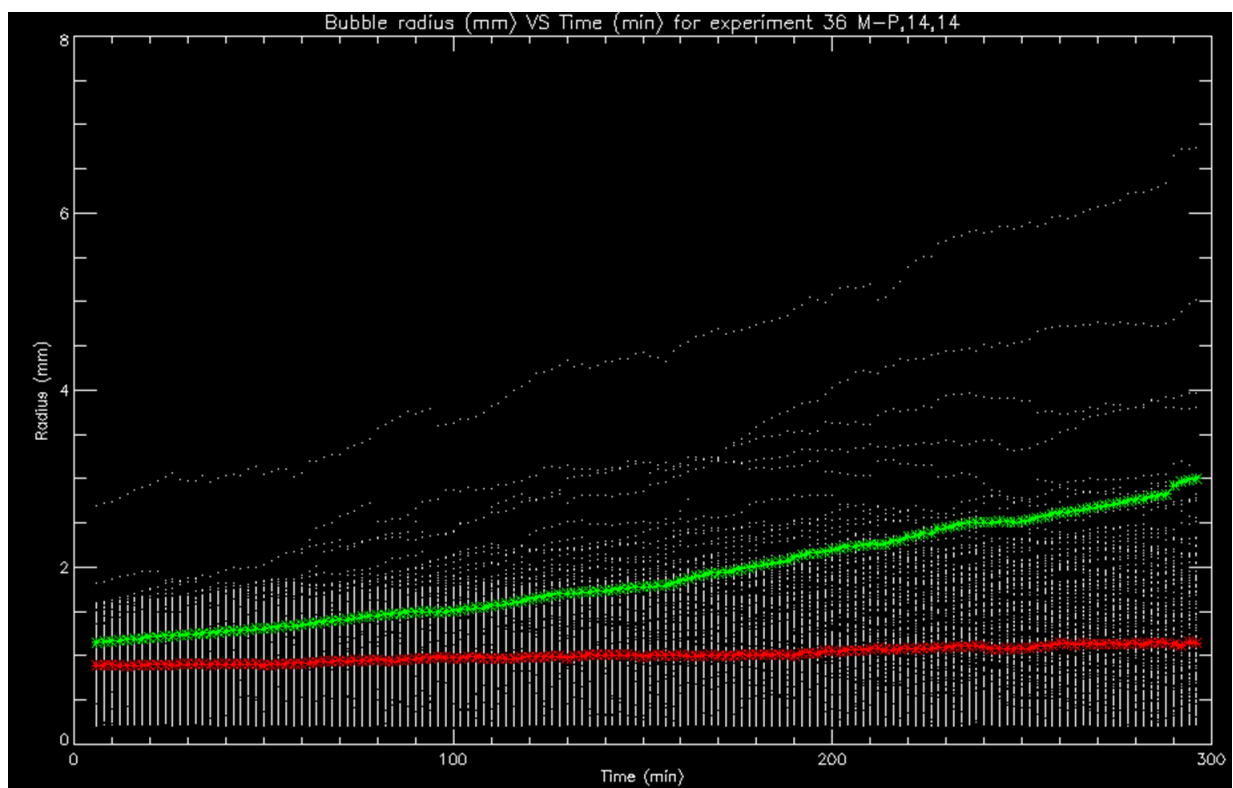
A big advantage when using the microfluidic foaming device over simply shaking the substance was the low polydispersity. Seen in Figure 22, there is an inherent divergent behavior between the large and small bubbles. Thus, over time the foam becomes more and more polydisperse. The polydispersity parameter is given by the following equation:

$$\text{Polydispersity} = \sqrt[3]{N} \frac{(\sum_n R_n^3)^{3/2}}{\sum_n R_n^2} - 1 = \frac{\langle R^3 \rangle^{2/3}}{\langle R^2 \rangle} - 1 \quad (4)$$

If the radii are the same, the polydispersity parameter is zero. Likewise, a polydispersity of one represents a reasonably strong polydispersity.

Another useful quantity is the number of bubbles tracked as a function of time. This number can be useful in determining the rupture rates and the corresponding

Figure 22: Individual bubbles through time



This shows a complete picture of the radius versus time of every bubble in experiment 36 using M-P,14,14 surfactant. Each dot is an individual bubble.

“half-life” of the bubbles.

4 Results

The Caran lab was successful with the synthesis of a wide family of amphiphiles. Because of the limited quantities of molecules, only four tricephalic amphiphiles were fully tested: M-1,14,14, M-P,14,14, M-1,1,14 and M-1,16,16. The foam these molecules produced was compared to foam stabilized by the three commercial, single tailed molecules: Cetyltrimethylammonium bromide (CTAB), Dodecyl trimethyl ammonium bromide (DTAB) and sodium dodecyl sulfate (SDS). It should be noted that several of the longer tailed tricephalic variants were insoluble in water and presumed useless in producing foam.

4.1 Sodium Dodecyl Sulfate (SDS)

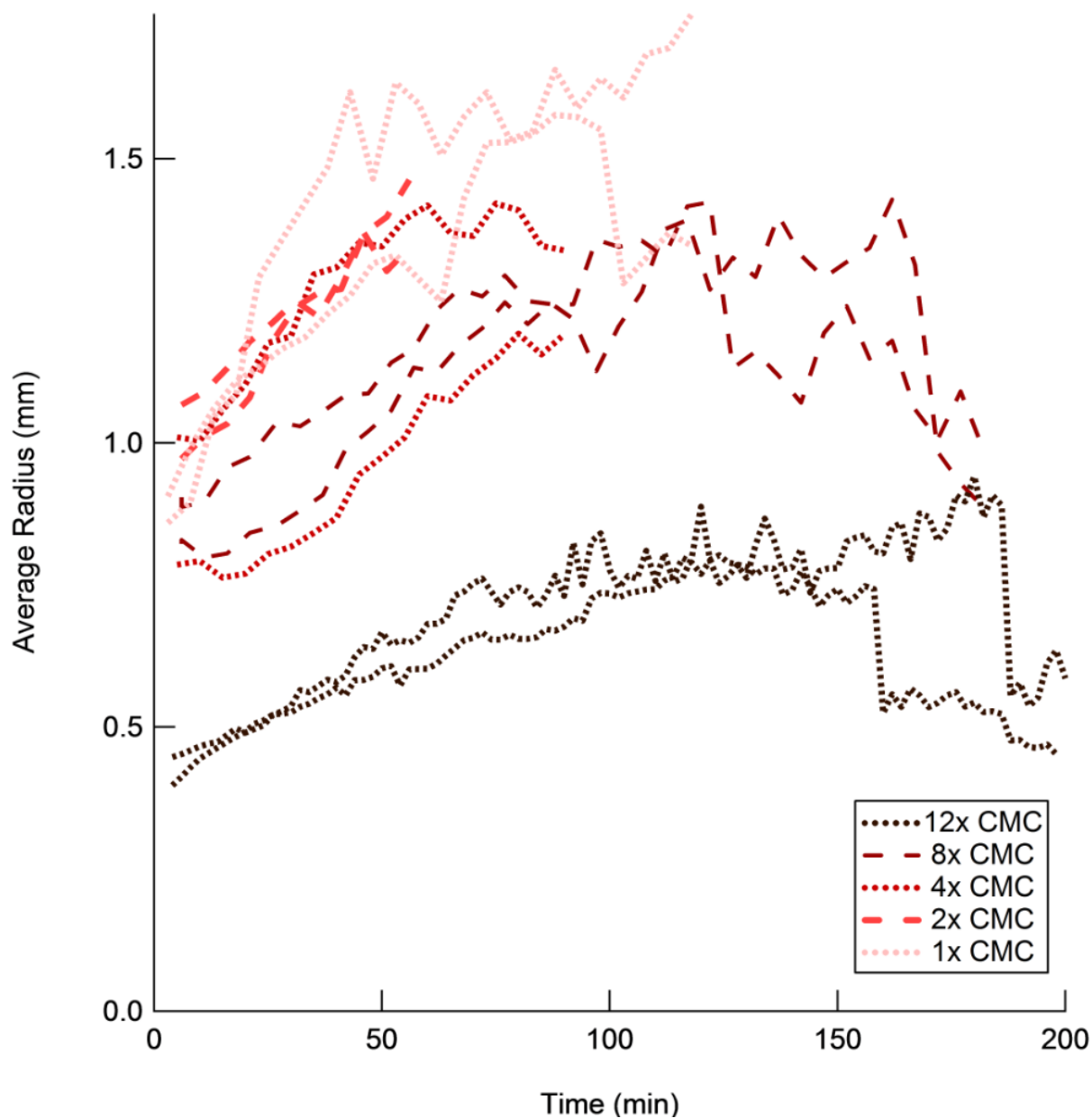
Due to its availability and common usage, the SDS molecule was extensively tested and acted as a test solution to find the best experimentation methods. Overall there were over a dozen experiments performed using SDS. These included the concentration tests with 12x, 8x, 4x, 2x and 1x CMC solutions as discussed earlier. Higher concentrations (up to 350x CMC, which was a gel) were also tested, however, 12.2x CMC worked as desired.

Figure 23 shows the average radius as a function of time for the tested concentrations. Not only were the coarsening rates different, but also the initial average size. The higher concentrations generally allowed smaller bubbles to be created. It should also be noted that in general, after $t = 150$ the data began to become inaccurate since the rupture of large bubbles dramatically affected the average size.

Figure 24 shows the corresponding rupture rates for experiments with different concentration of SDS molecules.

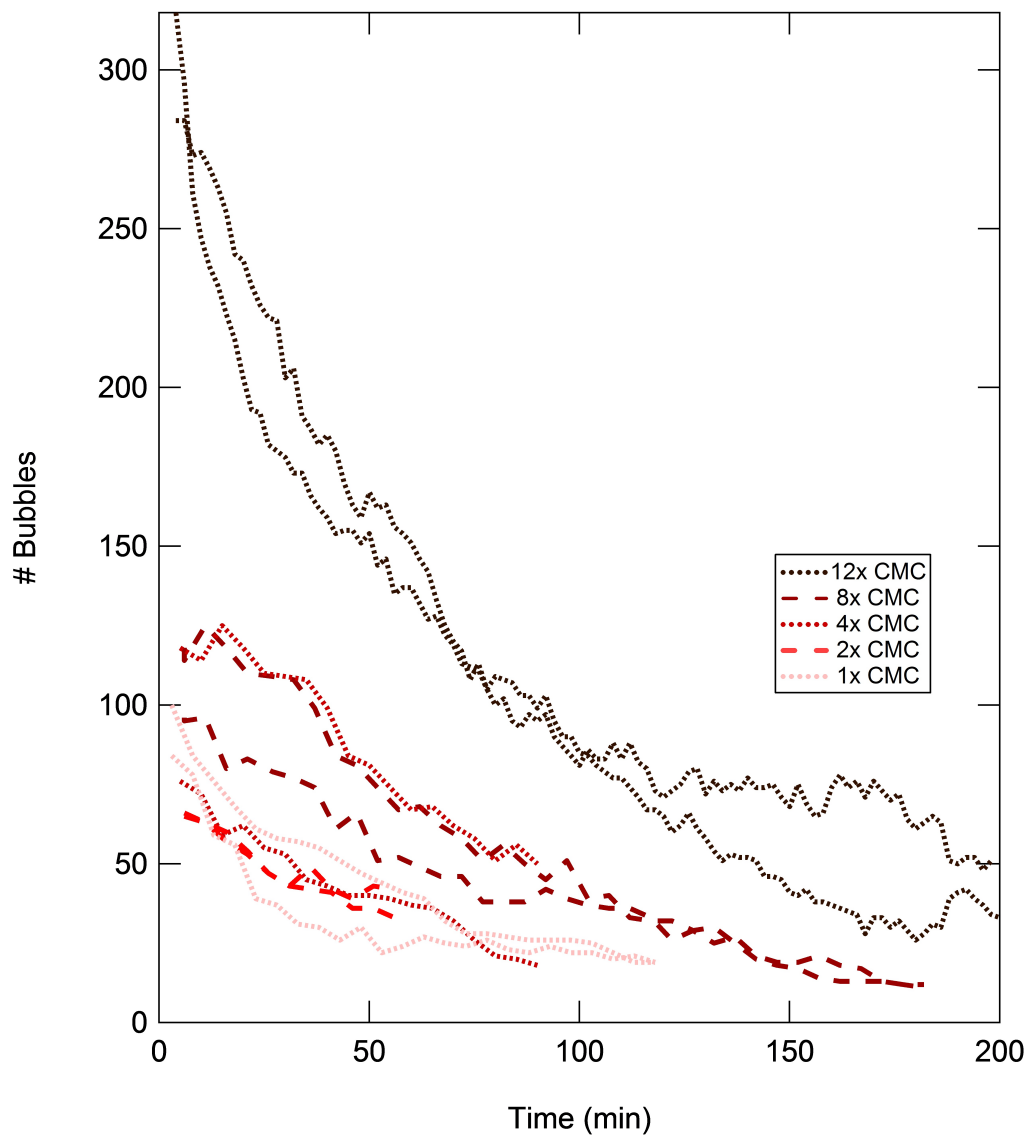
Once the 12.2x CMC was settled as the standard concentration, several experiments were performed. Figures 25, 26 and 27 show the bubble count, average Sauter radius and polydispersity respectively for SDS stabilized foam. It should be noted

Figure 23: Effect of different concentrations - average radius



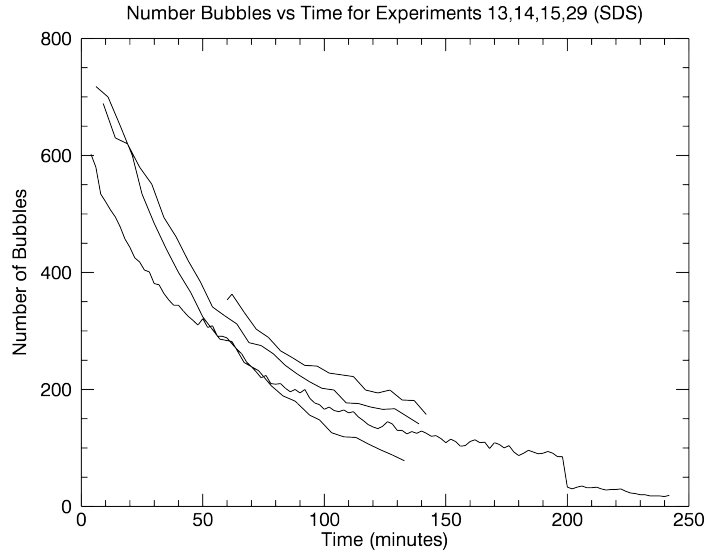
Average radius as a function of time for SDS created foam using solutions with concentrations ranging from 12.2x CMC to 1x CMC. Note that the 12x CMC displayed the slowest average growth, while the 1x expanded the quickest. The crashes in size (for example at $t = 160$, 12x CMC) can be explained by rupture of large bubbles; dramatically affecting the average size.

Figure 24: Effect of different concentrations - number of bubbles



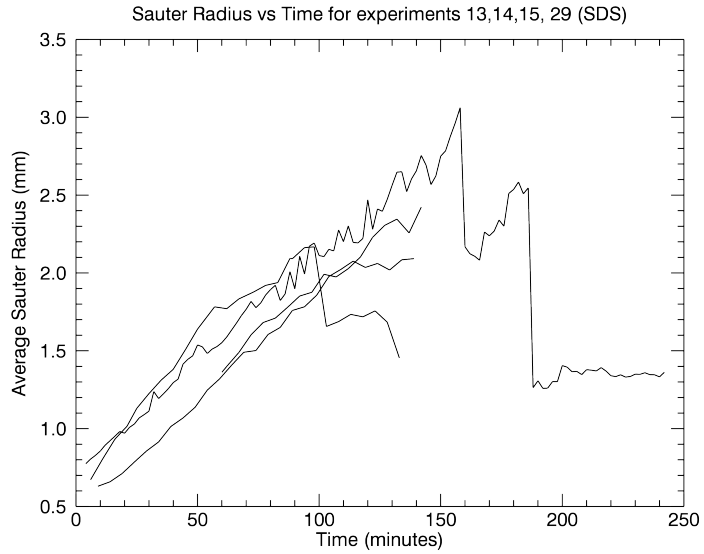
Number of bubbles as a function of time for SDS created foam using solutions with concentrations ranging from 1x to 12x CMC.

Figure 25: Bubble number for SDS



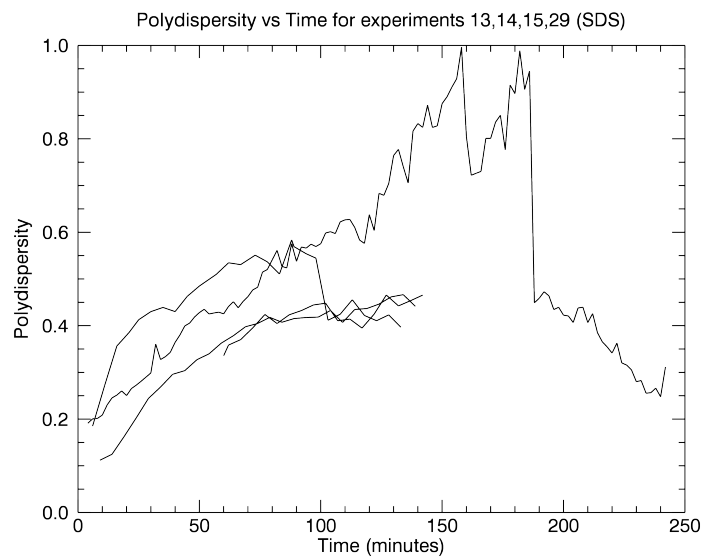
Bubble number vs time for all of the experiments using the SDS molecule (experiments 13, 14, 15 and 29).

Figure 26: Sauter radius for SDS



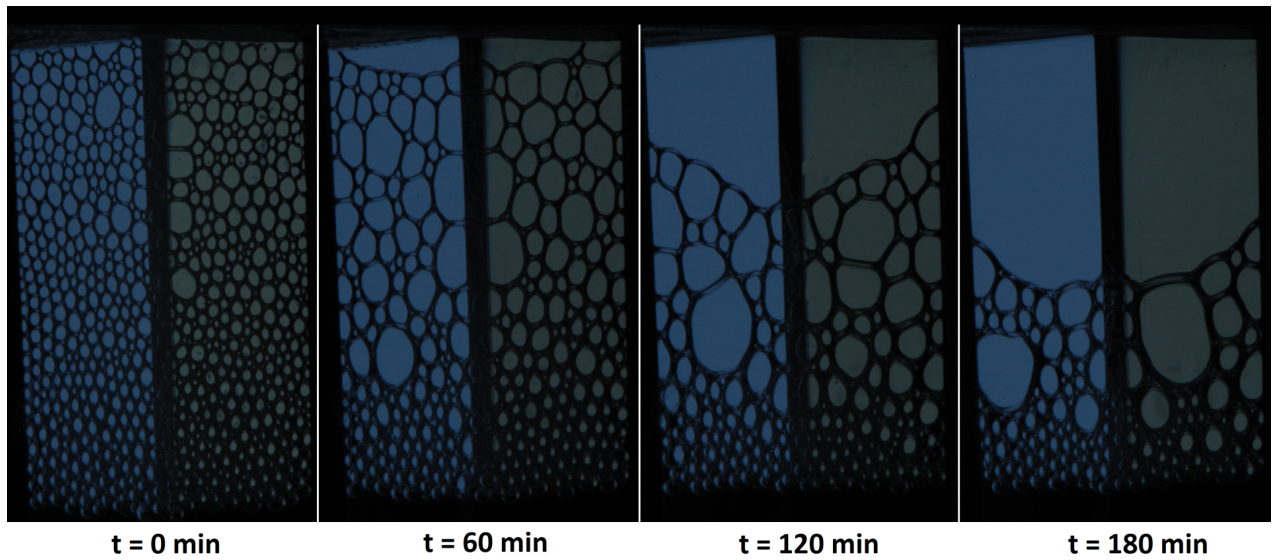
Average Sauter radius vs time for all of the experiments using the SDS molecule (experiments 13, 14, 15 and 29).

Figure 27: Polydispersity for SDS



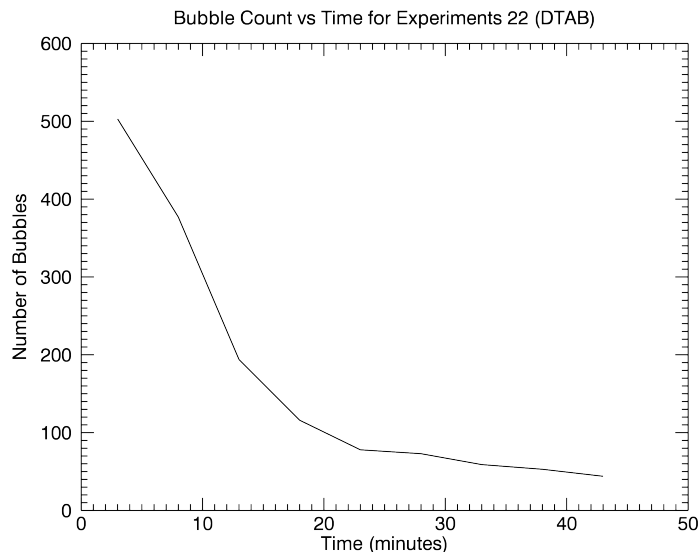
Polydispersity vs time for all of the experiments using the SDS molecule (experiments 13, 14, 15 and 29).

Figure 28: Foam evolution images for SDS



Sequence of SDS images (from experiment 29). Note the coarsening and the affect of capillary action.

Figure 29: Bubble number for DTAB



This plot displays the bubble number vs time using the DTAB molecule. Note the high rupture rate; almost all of the bubbles are gone after 30 minutes.

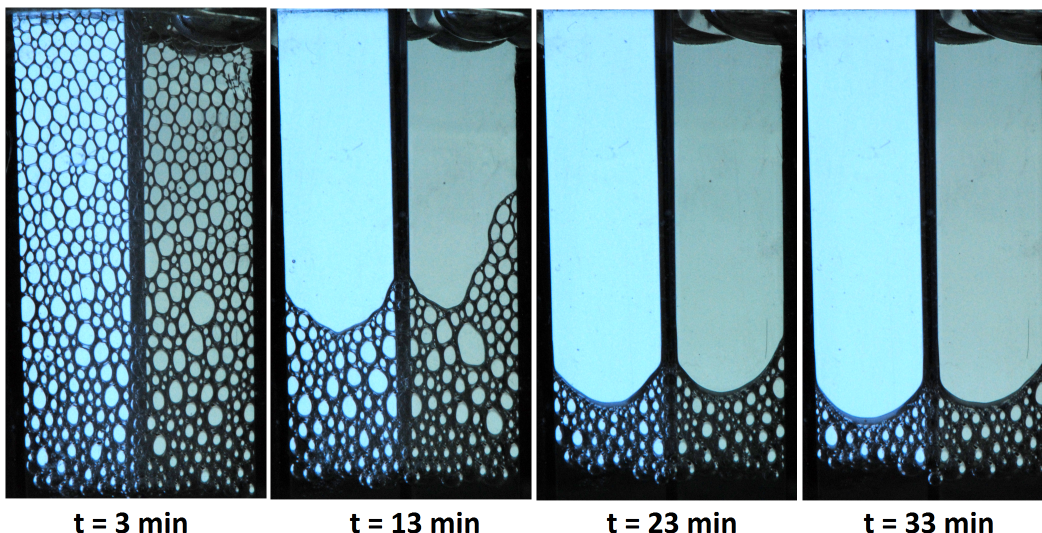
that since the number of bubbles decline with time, the error and fluctuations increase. With a small number of bubbles, a single bubble rupture or rearrangement can make a dramatic spike or decline in the data. An example of this is seen in Figures 26 and 27 when at about 160 minutes the polydispersity and average Sauter radius crash.

For a visual reference, Figure 28 shows four images (each an hour apart) of the evolving SDS foam.

4.2 Dodecyl Trimethyl Ammonium Bromide (DTAB)

The second commercial surfactant tested was DTAB. It was used along with CTAB, to compare the effects of tail length. The first thing to note about DTAB is its close molecular resemblance to SDS (See Figure 5). The differences include the head charge being positive instead of negative and it contains a sulfate group as head instead of a quaternary ammonium.

Figure 30: Foam evolution images for DTAB



Sequence of enhanced DTAB images (from experiment 22). Due to the high rupture rate, coarsening and polydispersity were indeterminate.

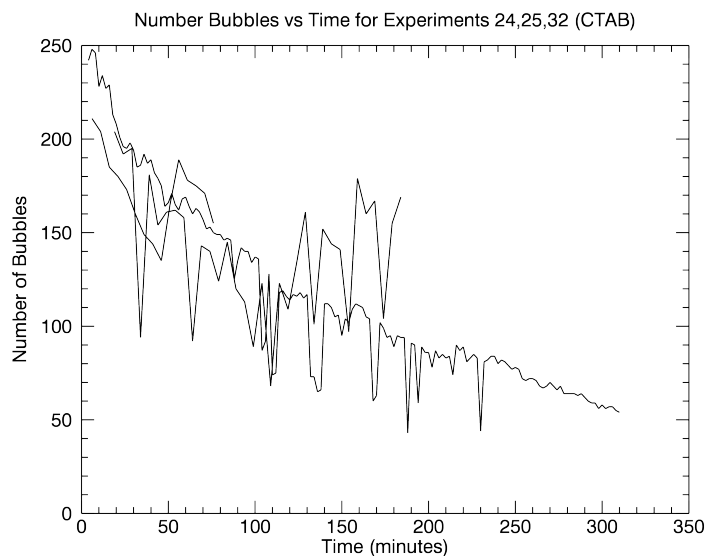
Using a solution of concentration 187 mM (12.2x CMC), foam using the DTAB surfactant was obtainable using the microfluidic device. Figure 29 shows the number of bubbles as a function of time. Note the high rupture rate. After about 30 minutes nearly all of the foam is gone. In fact, the ruptures of the bubbles could clearly be heard. Within about 5 minutes nearly half the original foam was gone, meaning the rupture rate was well above 300 pops a minute. The high rupture rate overshadowed the coarsening process and no meaningful coarsening data was collected. This can also be observed in the raw images.

Figure 30 show the raw images of experiment 22 at time 3, 13, 23 and 33 minutes respectively.

4.3 Cetyltrimethylammonium Bromide (CTAB)

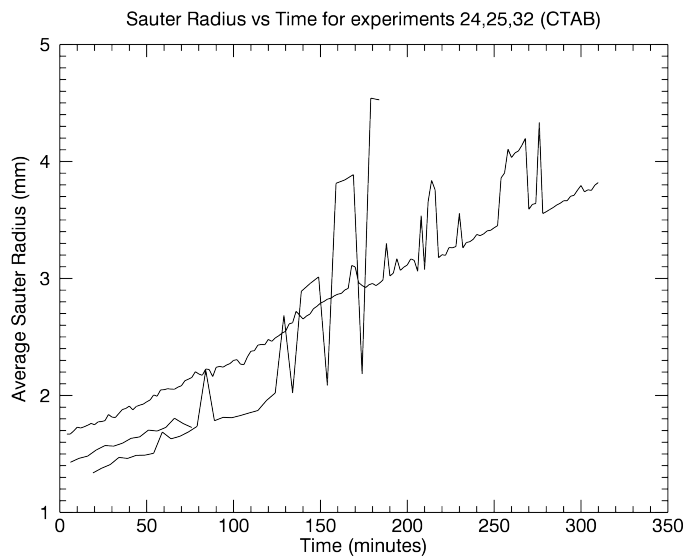
The DTAB and CTAB molecules are nearly identical with the only exception being the tail of CTAB having 16 hydrocarbons long as compared to DTAB with a tail only 12 hydrocarbons long (reference Figure 5). As seen in Figure 31, the longer

Figure 31: Bubble number for CTAB



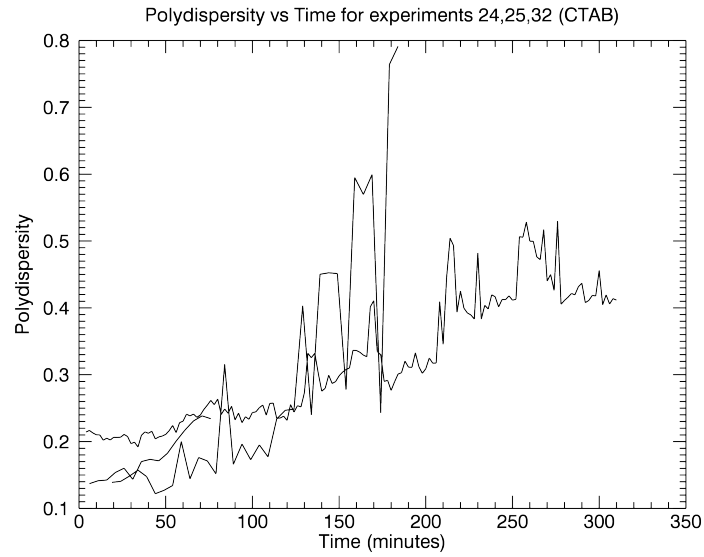
This plot displays the bubble number vs time for all of the experiments using the CTAB molecule (experiments 24, 25 and 32). The jumps in the line can be explained by the varying lighting of the image - a lighter image corresponds to an artificially high bubble count.

Figure 32: Sauter radius for CTAB



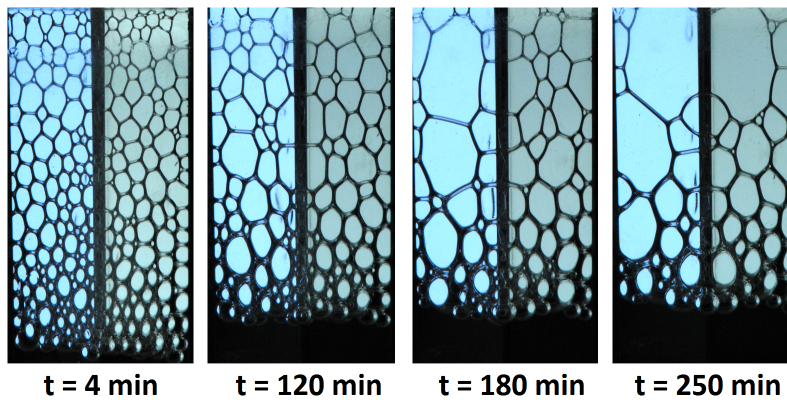
Average Sauter radius vs time for all of the experiments using the CTAB molecule (experiments 24, 25 and 32).

Figure 33: Polydispersity for CTAB



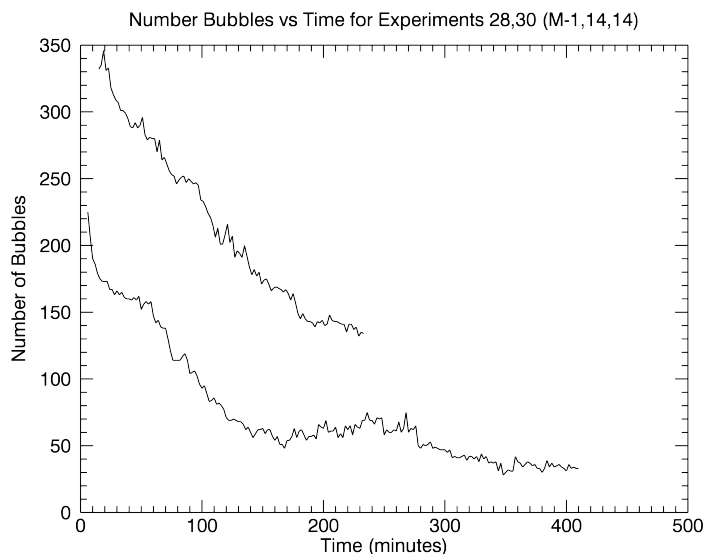
Polydispersity vs time for all of the experiments using the CTAB molecule (experiments 24, 25 and 32).

Figure 34: Foam evolution images for CTAB



Sequence of enhanced CTAB images (from experiment 32). Note the slow coarsening and absence of ruptures.

Figure 35: Bubble number for M-1,14,14



Bubble number vs time for all of the experiments using the M-1,14,14 molecule (experiments 28 and 30).

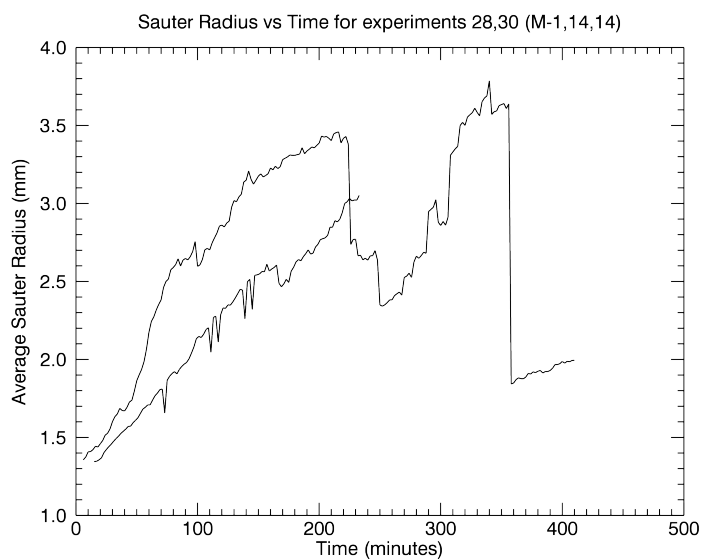
tail greatly improved the foam stability and decreased the rupture rate significantly. One puzzling trend was the large fluctuations in bubble count. There was one particular instance where the amount of bubbles sharply decreased by 50% and then jumped back to about the same number in a 2 minute period. These trends are discussed in detail in the “errors” section with the most likely cause being non-constant illumination and camera auto-focus.

The coarsening rate was also obtainable and is seen by the slow increase in Sauter mean radius, see Figure 32. The polydispersity for each of the CTAB experiments is seen in Figure 33. Figure 34 shows the raw images of experiment 28 at time 4, 120, 180 and 250 minutes respectively.

4.4 M-1,14,14

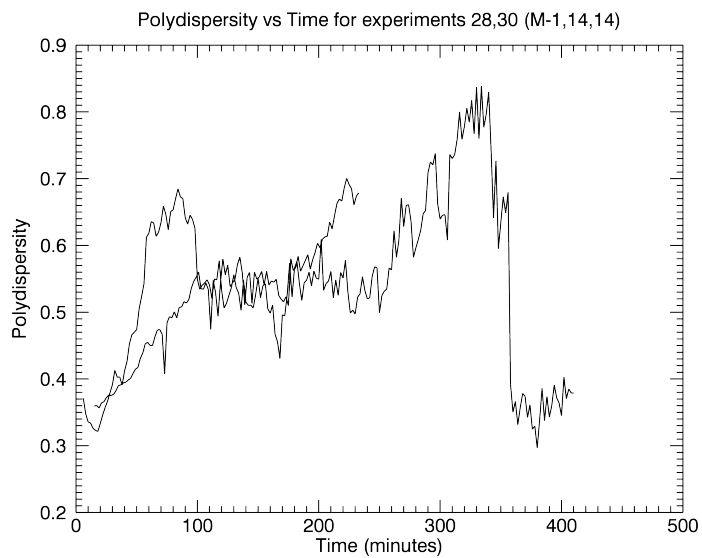
The M-1,14,14 amphiphile was chosen first since it reportedly exhibited foaming during synthesis. Because of its architecture, this molecule was difficult to compare

Figure 36: Sauter radius for M-1,14,14



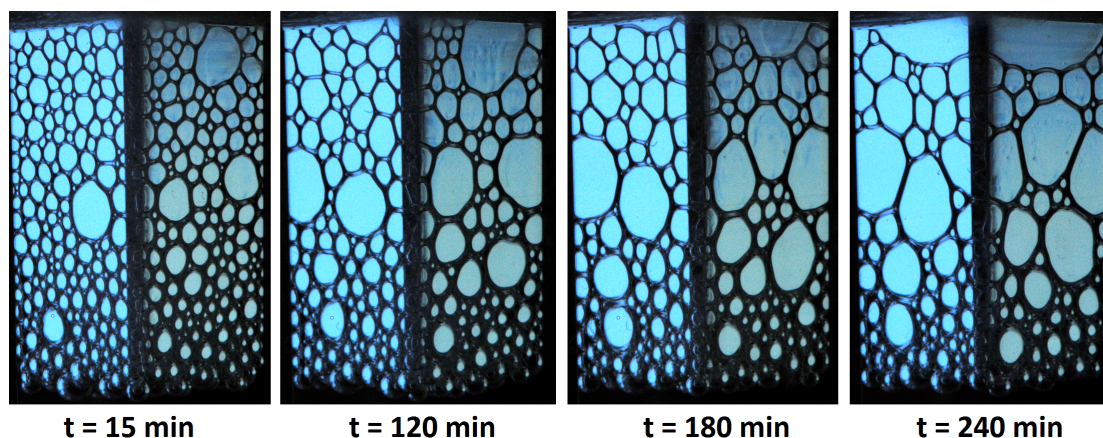
Average Sauter radius vs time for all of the experiments using the M-1,14,14 molecule (experiments 28 and 30).

Figure 37: Polydispersity for M-1,14,14



Polydispersity vs time for all of the experiments using the M-1,14,14 molecule (experiments 28 and 30).

Figure 38: Foam evolution images for M-1,14,14



Sequence of enhanced M-1,14,14 images (from experiment 30). Note the slow coarsening and absence of ruptures.

to CTAB, DTAB or SDS. The two tails are each 14 carbons long with a tricephalic head as displayed in Figure 4. The solution made with M-1,14,14 surfactant molecule shows excellent stability, lasting about just as long as those with the longer tailed CTAB surfactant (Figures 31 and 35). The Sauter mean radius and polydispersity also mirror these findings with a gradual increase in both. See Figures 36 and 37.

Figure 38 shows the raw images of experiment 30 at time 15, 120, 180 and 240 minutes respectively.

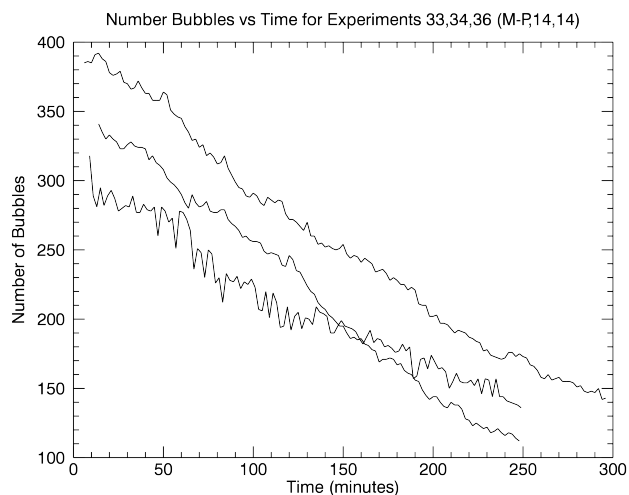
4.5 M-P,14,14

The M-P,14,14 and M-1,14,14 molecules were similar as seen in Figure 4. The key difference being the identity of the head with the M-P,14,14 molecule having a pyridinium group instead of a trimethylammonium.

The key difference that the M-P,14,14 molecule has about 4% more mass on the head. The hydrophilic charges and tail length were identical. These similarities proved important when comparing to the M-1,14,14 foam (reference Figures 39, 40 and 41).

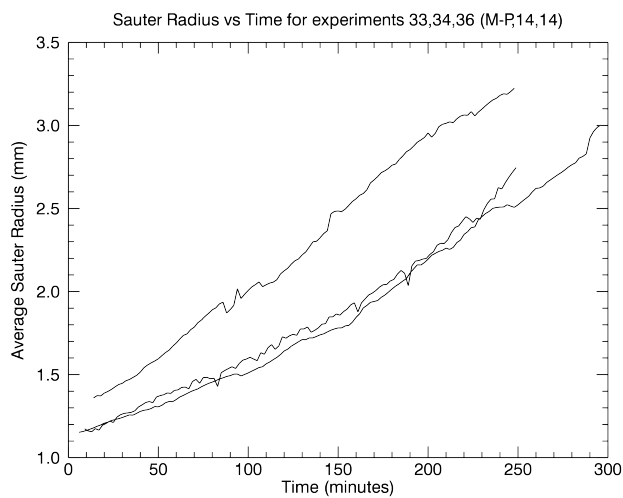
Figure 42 shows the raw images of experiment 36 at time 6, 100, 200 and 300

Figure 39: Bubble number for M-P,14,14



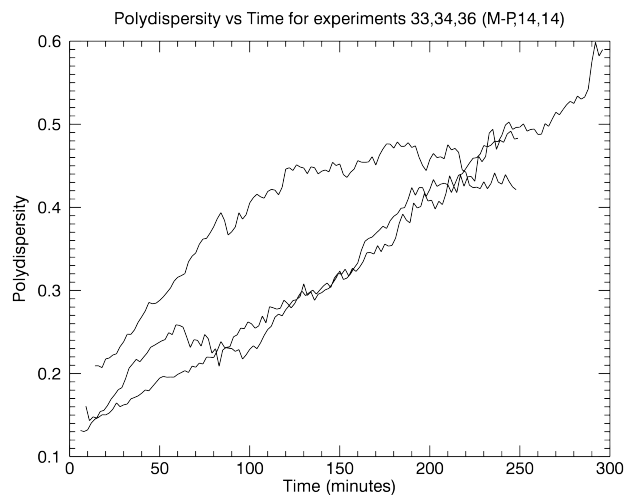
Bubble number vs time for all of the experiments using the M-P,14,14 molecule (experiments 33, 34 and 36).

Figure 40: Sauter radius for M-P,14,14



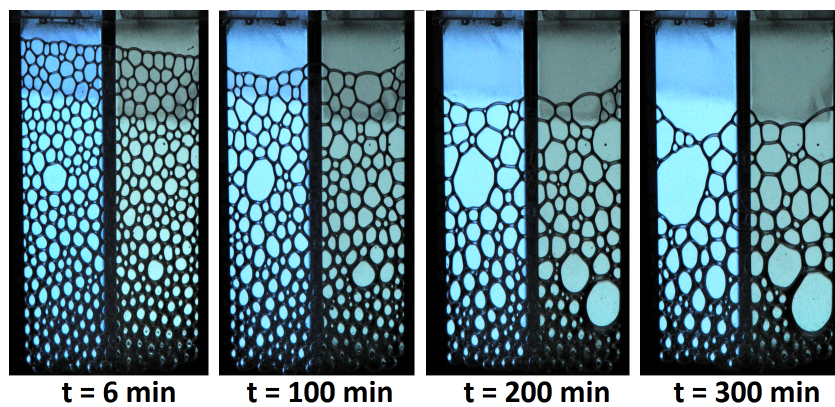
Average Sauter radius vs time for all of the experiments using the M-P,14,14 molecule (experiments 33, 34 and 36).

Figure 41: Polydispersity for M-P,14,14



Polydispersity vs time for all of the experiments using the M-P,14,14 molecule (experiments 33, 34 and 36).

Figure 42: Foam evolution images for M-P,14,14



This enhanced image shows a sequence of M-P,14,14 images (from experiment 36).

minutes respectively

4.6 M-1,16,16

The sharp contrast between the CTAB and DTAB stabilized foam show that tail length hugely affects the physics of foam. The M-1,16,16 molecules were identical to the M-1,14,14 with the exception of having a longer tail. We were unable to produce foam using the microfluidic device as the substance exiting the pipe would switch back and forth between spitting out liquid and air.

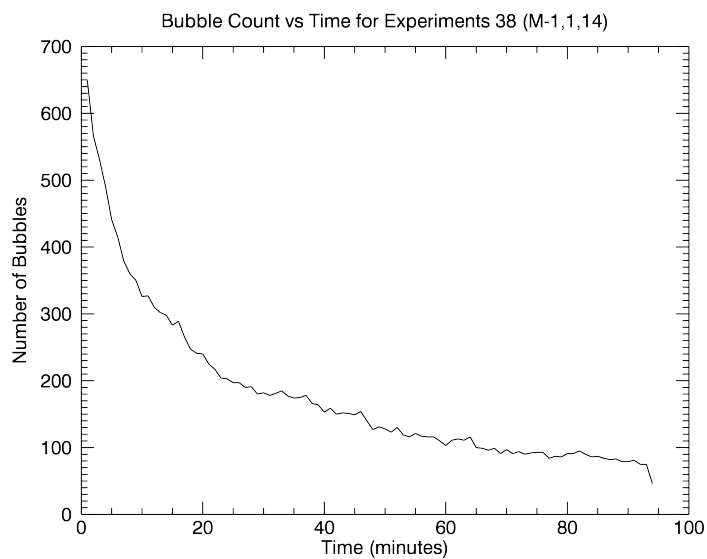
First we suspected that the concentration was not high enough. To fix this the concentration was doubled to 24.4x CMC. It should be noted that even though 24.4x CMC seems like a high concentration, it was actually still much lower than the M-1,14,14 surfactants (3.9 mM at 24.4x CMC of M-1,16,16 compared to M-1,14,14 at 7.4 mM at only 12.2x CMC). However, even with double the concentration, the foam could not be produced.

4.7 M-1,1,14

This molecule was identical to the M-1,14,14 surfactant with the exception of it having only one tail as seen in Figure 4. Since the CMC was about 35 times greater than any of the other surfactants (reference Figure 4), the amount of mass added was of close proportion to the amount of water added, thus, the fractional concentration was used to fix any inconsistencies between experiments.

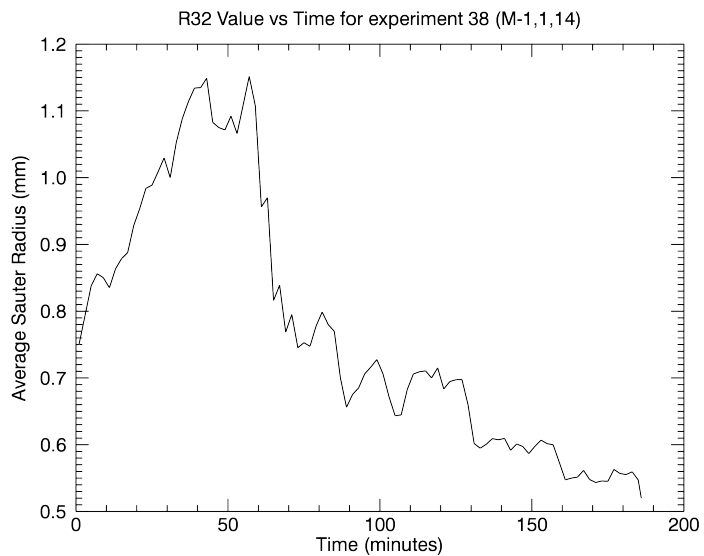
The lack of the extra tail affected the stability and foamability greatly. Due to its structure, the M-1,1,14 molecule proved difficult to produce foam using the microfluidic device. Instead, the cuvette was vigorously shaken to produce the foam seen in Figure 43. Despite this obstacle, the bubble decay was remarkably smooth (Figure 44) and somewhat resembled the curve seen with the SDS solution (Figure 25). Despite its high rupture rate, we were able to extract the Sauter mean radius of the M,1,1,14 stabilized foam seen in Figure 45. It is important to note that once most of the bubbles had dissipated, the calculated Sauter radius was meaningless and is the reason for the sharp divergence after about 50 minutes. Finally, Figure

Figure 43: Bubble number for M-1,1,14



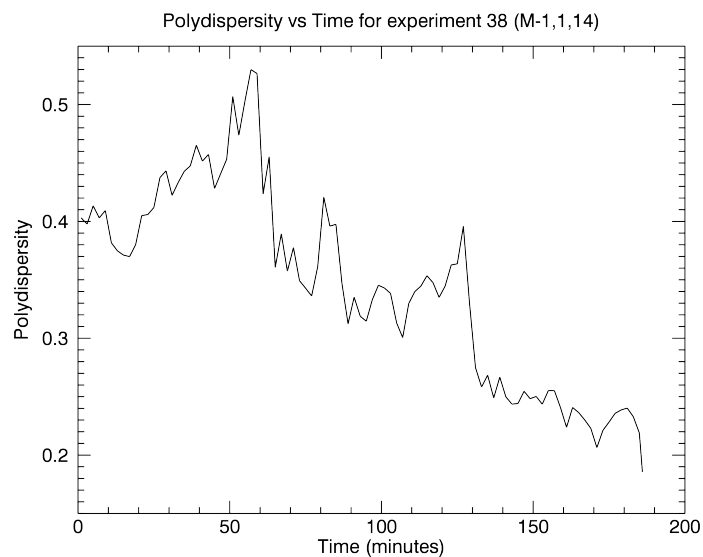
This plot displays the bubble number vs time for the M-1,1,14 molecule (experiment 38).

Figure 44: Sauter radius for M-1,1,14



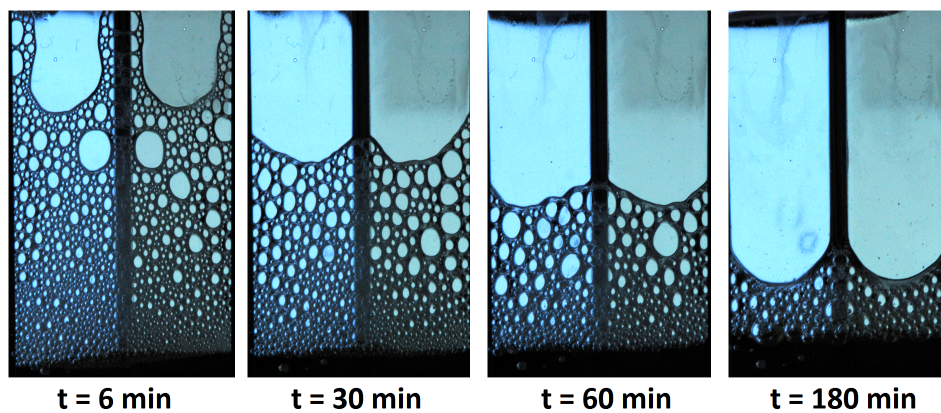
This plot displays the average Sauter radius vs time for the M-1,1,14 molecule (experiment 38).

Figure 45: Polydispersity for M-1,1,14



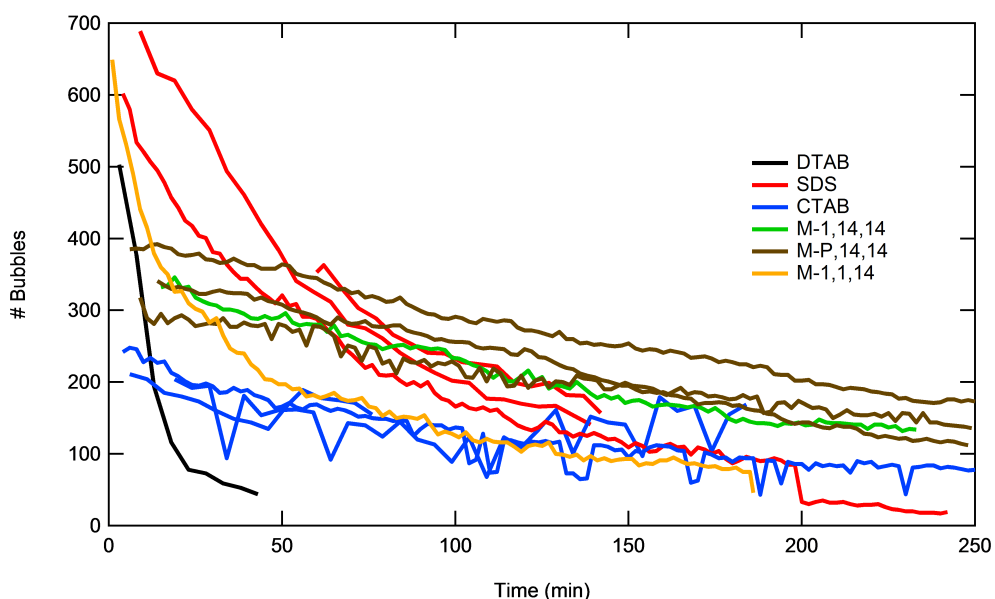
This plot displays the polydispersity vs time for the M-1,1,14 molecule (experiment 38). Note that this is the only surfactant to have a decreasing polydispersity, this is due to its poor stability. At first the polydispersity grows about the same rate as SDS, then begins to decline after about 30 minutes when most of the bubbles disappeared.

Figure 46: Foam evolution images for M-1,1,14



This enhanced image shows a sequence of M-1,1,14 images (from experiment 38).

Figure 47: Bubble number for all surfactants



Number of bubbles as a function of time for all of the different surfactants tested. An easy comparison can be made between unstable DTAB, M-1,1,14 and more stable CTAB. Multiple lines represent multiple experiments.

46 displays the polydispersity. Note the higher than average starting value of about 0.4. This is due to the method of foam production: vigorously shaking versus using the microfluidic device, this led to the high initial polydispersity.

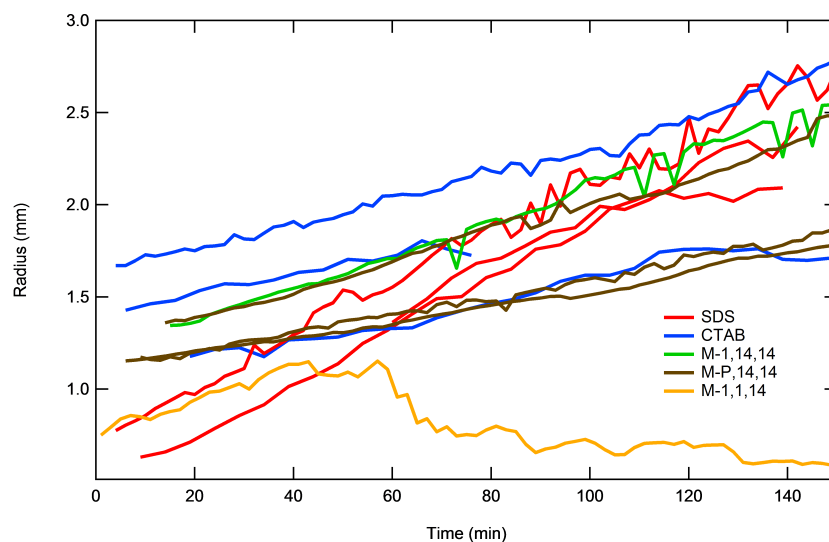
4.8 Comparing Results

Now is the point where the different surfactants can finally be compared against each other by looking at Figures 47, 48 and 49.

4.8.1 Bubble Count

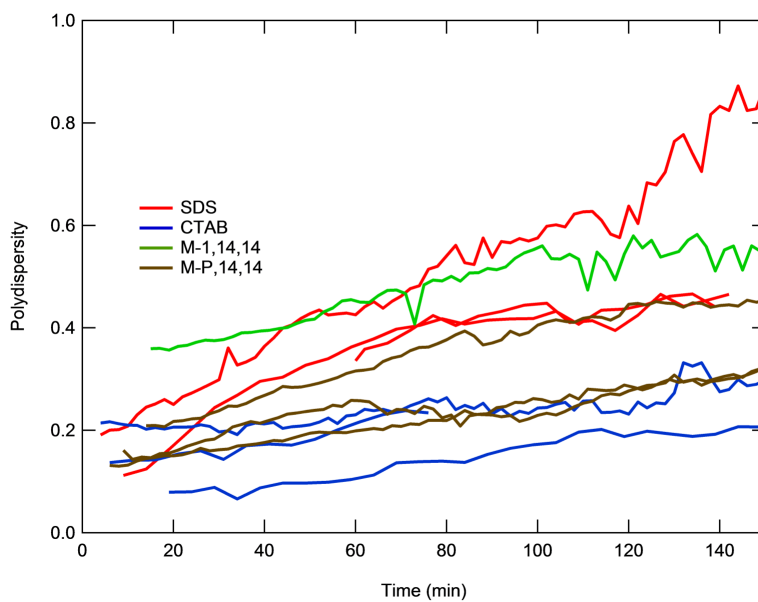
Figure 47 shows a graph including all of the most successful experiments for the number of bubbles as a function of time for each of the surfactants. The CTAB, M-1,14,14 and M-P,14,14 all show similar bubble number rates, CTAB lasting the longest of

Figure 48: Sauter radius for most surfactants



This plot shows the Sauter radius as a function of time for most of the different surfactants tested. Multiple lines represent multiple experiments.

Figure 49: Polydispersity for most surfactants



Polydispersity as a function of time for most of the different surfactants tested. Multiple lines represent multiple experiments.

all of the surfactants. Both of the shorter tailed surfactants, SDS and DTAB and the single tailed tricephalic, M-1,1,14 surfactant all showed a high decreases in the number of bubbles over time.

To clarify, it is important to see that there are two processes that dictate the bubble loss: coarsening and film rupture. Through coarsening, smaller bubbles vanish as the air moves to larger bubbles, film rupture usually is seen in larger, drier bubbles and commonly happens when there is less water stabilizing the surfactants. Thus it is possible that the curves seen in Figure 47 can be modeled on a composite of a negative exponential decay from the spontaneous film rupture (similar to radioactive decay) and a linear decrease given by small bubble vanishing through coarsening. This idea is given credit by observing the differences in the bubble count curves. The foam stabilized by CTAB (in blue) shows somewhat of a linear downward regression with hardly any rupture (see Figure 34). Conversely, foam stabilized by SDS or DTAB molecules (in red and black) show a negative exponential curve and a high apparent rupture rate as seen in Figures 28 and 30.

4.8.2 Coarsening and Polydispersity

Since the speed at which bubbles coarsen is related to the rate at which they grow/shrink, polydispersity and coarsening can be compared together. This fact is also seen by the similarities in Figures 48 and 49.

The coarsening rate and polydispersity, is seen in Figures 48 and 49 respectively. The SDS and M-1,1,14 foams shows nearly identical coarsening rates for the first 30 minutes before diverging. The other foams showed similar coarsening rates with the blue, CTAB surfactant solution having the slowest Sauter growth. The polydispersity mirrors these results with the CTAB consistently remaining the smallest and the SDS growing the quickest [†].

Figure 50 shows the results of the slope analysis. The Sauter slopes for each molecule tested are as follows: SDS 0.229 ± 0.003 , CTAB 0.117 ± 0.002 , M-1,14,14

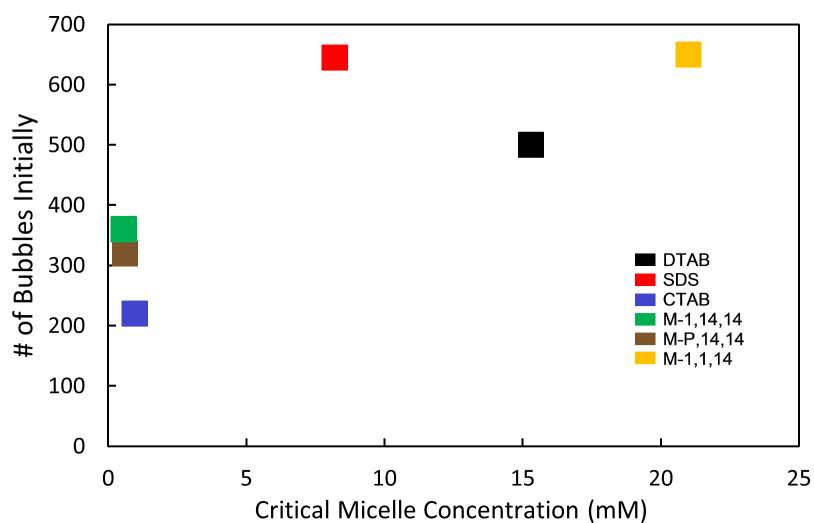
[†]The M-1,1,14 molecule was excluded in the polydispersity graph since it varied wildly and the data was unreliable.

Figure 50: Growth rates for each recorded surfactant

Name	Sauter Derivative ($\mu\text{m/s}$)
SDS	0.22897 ± 0.00280
CTAB	0.1173 ± 0.00178
M-1,14,14	0.1305 ± 0.00162
M-P,14,14	0.1214 ± 0.000849

The slopes of each of the surfactants' Sauter radius (Figure 49) with their corresponding error.

Figure 51: Number of initial bubbles versus Critical Micelle Concentration



Note the apparent trend: Higher CMC corresponds to a higher “foamability” questioning the integrity of the CMC and foamability link assumed in the experiment.

0.131 ± 0.002 , M-P,14,14 0.121 ± 0.001 . Note that the CTAB, M-1,14,14 and M-P,14,14 foams showed similar coarsening behavior.

4.9 Uncertainty and Assumptions

As discussed above, keeping all variables constant in order to effectively compare the different molecules proved challenging. By carefully controlling each variable and understanding its affect, greatly reduced error. However despite these efforts there was still several assumptions and areas for improvement.

Providing a consistent foamability was trickier than simply keeping variables such as concentration, polydispersity and initial bubble size constant. Although the 12.2x CMC provided a similar foamability, it was not constant. This fact can be observed by the size of the bubbles produced at the beginning of the experiments. SDS and DTAB foams seemed to have a high foamability since they produced the smallest bubbles initially. This inconsistency could have added error to any comparisons since concentration played a role in foam stability as seen in the SDS concentration experiments.

Other potential areas of error include the physical geometry of the bubbles (non-spherical), the experimental setup (only surface bubbles were observed) and computational limitations (noise and other artifacts could have been mistaken for a bubble). The following discusses these in a bit more detail:

- Because experiments were performed in a 3D container, sometimes bubbles would appear to grow extremely quickly when a large, out of sight bubble in the center of the cuvette, would shift outwards and into view.
- All bubbles smaller than 300 pixels were filtered out and the size of the pixel depended on the camera's distance from the sample. Thus, in experiments with the camera further away, more bubbles would have been filtered out before any data analysis.
- The bubbles were touching the glass, therefore, they couldn't be treated as perfect spheres. Thus, the radius calculations performed section 3.3 (Image

Analysis) are naturally slightly off.

- The liquid fraction (ϕ_{LF}) used (0.134) was constant throughout all experiments. This fraction could have had a varying effect on different solutions.

5 Conclusions

The original goal was to observe how the microscopic architecture of the foam molecules affected the stability and foamability. In this paper we were able to successfully study several physical properties of foam contained in a three dimensional cuvette. We first streamlined a process to produce and study a SDS stabilized foam, after this was done we moved on to test the foaming properties of other single and tricephalic head groups.

There are several ways in which the foamability of a foam can be correlated with its corresponding molecular properties. The molecular properties tested in this experiment are as follows: Critical micelle concentration (CMC), number of tails, magnitude of charge of head group and the tail length.

Initially we assumed the CMC was directly correlated with foamability. Our findings show that while the CMC does seem to affect foamability, there are several other variables at play. In order for foam formation to happen, the surfactants must be able to absorb at liquid-air interfaces. At a low CMC, the amphiphilic molecules reach a solubility limit. This causes a decrease in molecular mobility, decreasing the surfactant's ability to absorb dynamically at the interfaces. This hinders foamability since there are less surfactant molecules available to stabilize foam. The longer tailed M-1,16,16 exhibited this behavior with its low foamability. Thus in the limited regime tested, a higher CMC will result in foam that is easier to produce.

Since the CMC is generally inversely proportional to the tail length, it will also be inversely proportional to that molecule's foamability. This makes sense conceptually since shorter tailed molecules (generally higher CMC) are more likely to absorb at interfaces than form micelles, this allows them to be more foamable.

The tail count also makes a big difference, this can be seen when comparing

the M,1,14,14 (double tailed) and M,1,1,14 (single tailed) stabilized foams. With an extra tail, the molecules may absorb along interfaces easier resulting in a higher foamability.

Another area of comparison is the head group charge. Single charged head groups found in the CTAB, and DTAB molecules exhibited high foamability in comparison to the tricephalic (triple headed) molecules. The best comparison comes from the DTAB and M-1,1,14 molecules. Despite having similar tail length, CMC and tail count, the DTAB molecules were still significantly more foamable. Due to its charge, it will exhibit a greater attraction to water and thus, be less attracted to liquid-air interfaces (lower foamability).

Thus from our findings, the structure of the most foamable foam would have a high tail count, high CMC, shorter tail and a small head group charge.

Looking at stability, there is a large difference between foamability and stability. For example, the DTAB foam was easy to produce (high foamability) but dissipated very quickly, conversely, CTAB was more difficult to produce, yet, lasted longer than 4 hours (high stability). The key difference between these two is the tail length. Thus it seems that while harder to produce, foam using longer tailed surfactants seem to remain stabilized much longer than shorter tailed, highly foamable surfactants.

The head group identity did not seem to affect the stability (M-1,14,14 vs M-P,14,14), however, it could be argued that this difference was insignificant and any correlation could have been lost in the error.

We also report a huge difference in stability when looking at tail count with the removal of one hydrocarbon tail having a huge effect on the stability (M-1,14,14 vs M-1,1,14).

The length of the tail had a huge impact on rupture rates. This is clearly seen in comparison between CTAB and DTAB. The two molecules differentiated only by their tail lengths: CTAB having a tail length of 16 and DTAB with a shorter length tail of 12 hydrocarbons.

A less strong connection seems to exist between the coarsening rates and tail length. The SDS stabilized foams showed a much faster coarsening rate than the longer tailed CTAB, M-1,14,14 and M-P,14,14. As seen by comparing the SDS and

DTAB, it is clear that other factors such as head charge are at play. However, there is a general trend (with the exception of the single tailed M-1,1,14) that the longer tailed molecules have slower coarsening rates. A possible explanation for this trend is that for longer tailed surfactants the bubble films would be thicker and air would diffuse more slowly. In this way foam made with longer tailed surfactants would last much longer.

The rupture rate dependence is trickier. Rupture happens when the films get too thin and the surfactant molecules cannot retain their alignment. A medium length tail may have a way of stabilizing this alignment, preventing the surfactants from flipping over. Conversely, foam stabilized with longer tails may have difficulty absorbing at the interfaces from the beginning. This was seen with the M-1,16,16 molecule's difficulty in stabilizing foam.

6 Outlook

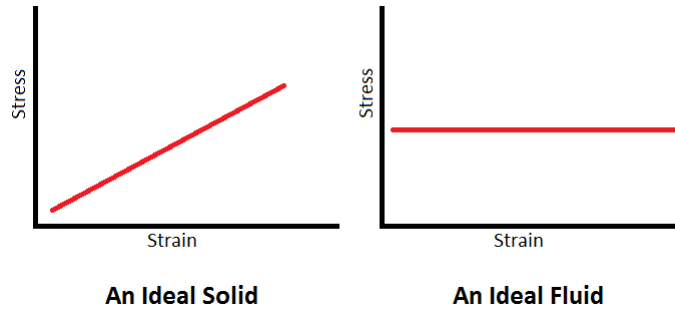
This paper gives a detailed analysis of the experimental methods involved in testing foam stabilized by tricephalic amphiphiles. Several simple areas of experimental improvement are indeed possible. By using an improved time resolution, bubble tracking may become a possibility allowing a better understanding of size. Using a larger cuvette would improve accuracy. Testing different surfactant concentrations beyond the 12.2x CMC, allowing for a better understanding of "foamability." Other areas of further experimentation include better understanding how shorter tail lengths or different head structures affects foam evolution. This could be done by studying the M-1,12,12 molecule's foamability and/or testing bicephalic (double headed) surfactant molecules.

In addition to discovering areas of potential improvement, this study has also uncovered new questions. One question: "If the CMC does not dictate 'foamability' then what does?" Answering this question would be a key area of future work.

Overall, this study further examines three dimensional foam properties. The general applications for this research are boundless due to the high usage of foam in our everyday life. Understanding how molecular architecture affects foam evolution

allows a better engineering of a desired foam. More immediate applications can be realized by taking advantage of the unique antibacterial properties of the multi-
cephalic surfactants. By combining this with the cleaning properties of foam, an effective cleaning product may be a possibility. The foaming nature may also be applicable in situations where the molecules need to stick to a surface, thus a foaming spray might be useful.

Figure 52: Ideal Solids and Fluids



Left: An ideal, elastic-like solid. The stress is linearly proportional to the strain. **Right:** An example of a Newtonian fluid, when a constant stress is applied the fluid will “flow” at a constant strain rate.

Appendix: Solids, Newtonian Fluids and Complex Fluids

Rheology is the study of how fluids and solids behave when stressed [5]. There is a distinct rheological difference between solids and liquids. An ideal solid, when strained, will build up energy similar to a spring and when relieved, it will bounce back. Fluids in which do not show elastic properties and instead yield continuously under shear stresses are known as Newtonian liquids [6]. Fluids also do not “remember” their position and their stress level remains the same regardless of how far they are strained. This distinction can be seen in the stress versus strain plots shown in Figure 52.

The graphs shown in Figure 52 represent “ideal solids,” where Hooke’s Law holds perfectly, and Newtonian fluids, where the strain rate $\dot{\gamma}$ is perfectly proportional to the stresses applied σ [7,8]. This can be described by the following relation:

$$\sigma = \frac{\partial v_x}{\partial y} = \eta \dot{\gamma} \quad (5)$$

With σ being the stress, the proportionality constant η being viscosity and $\dot{\gamma}$ as the strain rate [9].

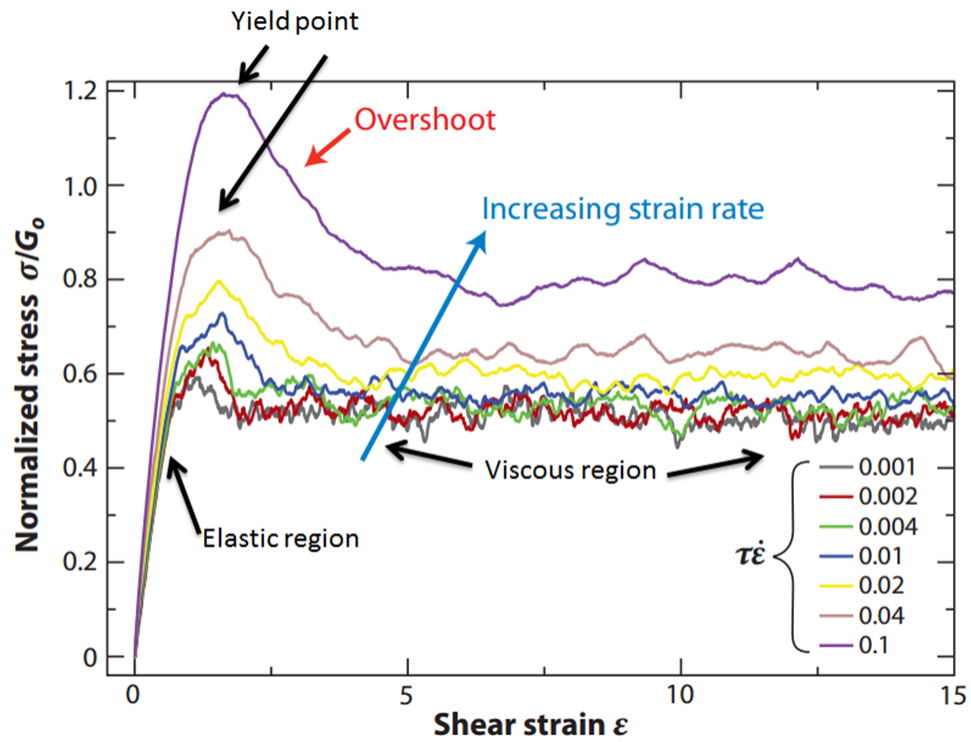
Many fluids do not fit these “perfect” models, with the viscosity η being non-constant. These fluids are known as non-Newtonian or complex fluids. Everyday substances such as mayonnaise, milk, non-drip paint, or toothpaste are examples of these non-linear or complex fluids.

This paper focuses on foam, which is a complex fluid. When compared to the simple behavior Figure 52, foams exhibit a non-linear, discontinuous, or even a combination of both behaviors.

It is important to note that “foam” can be used to describe many different things, for example, shaving cream, bread, foam insulation and ice cream. However, for simplicity of this paper the term “foam” will refer to aqueous foam, that is, foam stabilized purely by surfactant molecules and liquid substances alone with no stabilizing minerals or polymers added [10].

Foam, or any complex fluid, displays interesting rheology and possesses a duality of solid-like and liquid-like properties. Stressed, foams tend to possess a Hookian line, however, when foam is strained enough, it will yield and fluidize behaving similar to a Newtonian fluid [9]. A stress versus strain graph of this dual behavior is seen in Figure 53.

Figure 53: A Complex Fluid



This plot displays the normalized stress versus strain of Gillette shaving cream (Source: Khan et al, 1988), note the dual behavior: Initially the foam exhibits a Hookian trend, however, at a certain point the foam yields and “fluidizes” behaving more like a Newtonian fluid.

References

- [1] Roszak, K., Torcivia, S., Hamill, K., Hill, A., Radloff, K., Crizer, D., Middleton, A., Caran, K. (2008). Biscationic bicephalic (double-headed) amphiphiles with an aromatic spacer and a single hydrophobic tail. *Journal of Colloid and Interface Science*. 331(2), 560-564. doi:10.1016/j.jcis.2008.12.014
- [2] Wales - The birthplace of Flotation. (2009). Retrieved from <http://www.maelgwyn.com/birthplaceflotation.html>.
- [3] Caran Lab. James Madison University Department of Chemistry and Biochemistry. Unpublished work, publication expected Q3 2015.
- [4] LaDow, J., Warnock, D., Hamill, K., Simmons, K., Davis, R., Schwantes, C., ... Seifert, K. (2011). Bicephalic amphiphile architecture affects antibacterial activity *Eur J Med Chem*. (46). 4219-4226).
- [5] Daniel T.N. Chen, Qi Wen, Paul A. Janmey, John C. Crocker, and Arjun G. Yodh. (2010). Rheology of Soft Materials. *Annual Review of Condensed Matter Physics*. 1:301-22.
- [6] Hunter, G and Weeks, E. (2011). The physics of the colloidal glass transition. *Reports on Progress In Physics*. 75(6). 30pp. doi:10.1088/0034-4885/75/6/066501
- [7] Batchelor, G. (1970). An Introduction to Fluid Dynamics. Cambridge: *Cambridge University Press*.
- [8] Czarnota, M., & Thomas, P. (2013). Using Surfactants, Wetting Agents, and Adjuvants in the Greenhouse. Retrieved from http://extension.uga.edu/publications/files/pdf/B_1319_5.PDF
- [9] P. S. Piispanen, (2002), Synthesis and Characterization of Surfactants Based on Natural Products, Thesis, Kungl Tekniska Hogskolan. Stockholm.

- [10] Halliday, H. (2008). Surfactants: Past, present and future. *Journal of Perinatology*. (28).
- [11] D, J. (1997, May). Understanding foams and foaming. *University of Minnesota*.
- [12] Pugh, R. (2005). Experimental techniques for studying the structure of foams and froths. *Advances in Colloid and Interface Science*. (115). 239-251. doi:10.1016/j.cis.2004.08.005
- [13] Erni, P. (2011). Deformation modes of complex fluid interfaces. *Soft Matter*. (7). 7586-7600.
- [14] F, Fan. K, Yan. N, Wallis. S, Reed. T, Moore. S, Rittenhouse. W, DeWolf Jr.. J, Huang. D, McDevitt. W, Miller. M, Seefeld. K, Newlander. D, Jakas. M, Head. D, Payne. (2002). Defining and combating the mechanisms of triclosan resistance in clinical isolates. *Antimicrobial Agents and Chemotherapy*. (46). doi: 10.1128/AAC.46.11.3343-3347.2002.
- [15] A, S., M, I., Emile, J., & A, S. (2010). Solutions of surfactant oligomers: a model system for tuning foam stability by the surfactant structure. *Soft Matter*. 10(1039).
- [16] Pugh, R.J. (2005). Experimental techniques for studying the structure of foams and froths. *Advances in Colloid and Interface Science*. 114-115:239-51.
- [17] P. Mukerjee and K. J. Mysels. (1971). "Critical Micelle Concentration of Aqueous Surfactant Systems." NSRDS-NBS 36. US. Government Printing Office. Washington, D.C.
- [18] Roth, A., Chen, B., & Durian, D. (2013). Structure and coarsening at the surface of a dry three-dimensional aqueous foam. ArXiv, 1306.2939 [cond-mat.soft].
- [19] Feitosa, K., & Durian, D. (2007). Gas and liquid transport in steady-state aqueous foam. *The European Physical Journal E*. (26). 309-316.